Cell

Species-Dependent Posttranscriptional Regulation of *NOS1* by FMRP in the Developing Cerebral Cortex

Kenneth Y. Kwan,[1] Mandy M.S. Lam,[1] Matthew B. Johnson,[1] Umber Dube,[1] Sungbo Shim,[1] Mladen-Roko Rašin,[1,2] André M.M. Sousa,[1,3] Sofia Fertuzinhos,[1] Jie-Guang Chen,[1,4] Jon I. Arellano,[1] Daniel W. Chan,[1] Mihovil Pletikos,[1,5] Lana Vasung,[5] David H. Rowitch,[6] Eric J. Huang,[7] Michael L. Schwartz,[1] Rob Willemsen,[8] Ben A. Oostra,[8] Pasko Rakic,[1] Marija Heffer,[9] Ivica Kostović,[5] Milos Judaš,[5] and Nenad Šestan[1,*]

[1]Department of Neurobiology and Kavli Institute for Neuroscience, Yale University School of Medicine, New Haven, CT 06510, USA
[2]Department of Neuroscience and Cell Biology, University of Medicine and Dentistry of New Jersey/Robert Wood Johnson Medical School, Piscataway, NJ 08854, USA
[3]Graduate Program in Areas of Basic and Applied Biology, Abel Salazar Biomedical Sciences Institute, University of Porto, Porto 4099-002, Portugal
[4]School of Optometry and Ophthalmology, Wenzhou Medical College, Wenzhou, Zhejiang 325003, China
[5]Croatian Institute for Brain Research, University of Zagreb School of Medicine, Zagreb 10000, Croatia
[6]Departments of Pediatrics and Neurosurgery, Eli and Edythe Broad Institute for Stem Cell Research and Regeneration Medicine and Howard Hughes Medical Institute
[7]Department of Pathology
University of California, San Francisco, San Francisco, CA 94143, USA
[8]Department of Clinical Genetics, Erasmus MC, Rotterdam 3000 CA, The Netherlands
[9]Department of Medical Biology, Josip Juraj Strossmayer University of Osijek, Osijek 31000, Croatia
*Correspondence: nenad.sestan@yale.edu
DOI 10.1016/j.cell.2012.02.060

SUMMARY

Fragile X syndrome (FXS), the leading monogenic cause of intellectual disability and autism, results from loss of function of the RNA-binding protein FMRP. Here, we show that FMRP regulates translation of neuronal *nitric oxide synthase 1* (*NOS1*) in the developing human neocortex. Whereas *NOS1* mRNA is widely expressed, NOS1 protein is transiently coexpressed with FMRP during early synaptogenesis in layer- and region-specific pyramidal neurons. These include midfetal layer 5 subcortically projecting neurons arranged into alternating columns in the prospective Broca's area and orofacial motor cortex. Human *NOS1* translation is activated by FMRP via interactions with coding region binding motifs absent from mouse *Nos1* mRNA, which is expressed in mouse pyramidal neurons, but not efficiently translated. Correspondingly, neocortical NOS1 protein levels are severely reduced in developing human FXS cases, but not FMRP-deficient mice. Thus, alterations in FMRP posttranscriptional regulation of *NOS1* in developing neocortical circuits may contribute to cognitive dysfunction in FXS.

INTRODUCTION

The development of neural circuits is a precisely regulated process susceptible to genetic alterations that can lead to disorders affecting the most distinctively human aspects of cognition, including speech and language, theory of mind, and complex social behavior (Geschwind and Levitt, 2007; Lui et al., 2011; Ramocki and Zoghbi, 2008; State, 2010; Walsh et al., 2008). One such disorder, fragile X syndrome (FXS), is the leading inherited cause of intellectual disability and is often accompanied by autistic-like features, aggression, attention deficits, and delays in speech and language development (Abbeduto et al., 2007; Rogers et al., 2001; Willemsen et al., 2011). FXS is caused by loss of function of the *FMR1* gene, which encodes an RNA-binding protein (FMRP) involved in mRNA localization, stability, and translation (Ashley et al., 1993; Bagni and Greenough, 2005; Bassell and Warren, 2008; Zalfa et al., 2007). Many FMRP mRNA targets function in synaptic development and plasticity (Brown et al., 2001; Darnell et al., 2011). Concordantly, *Fmr1*-deficient mice show neural deficits also found in patients with FXS (The Dutch-Belgian Fragile X Consortium, 1994). However, FMRP target mRNAs and their role in human neurodevelopment are not as well understood.

The study of human FMRP function may also provide insights into the molecular mechanisms and neural circuits affected in autism spectrum disorders (ASDs), which are highly comorbid with FXS (Rogers et al., 2001). ASDs are a group of complex developmental syndromes characterized by impairments in social communication and language development, and repetitive behaviors. Multiple lines of evidence point to the dysfunction of neocortical circuits involved in social, emotional, and language processing in ASDs (Geschwind and Levitt, 2007; State, 2010; Walsh et al., 2008). Although no overt neuroanatomical alterations have been linked to the autistic brain, there is emerging evidence of abnormal organization of cortical minicolumns

(Casanova et al., 2002; Peters, 2010), which are composed of vertically arranged neurons connected into a local network and thought to originate from developmental radial units (Mountcastle, 1997; Rakic, 1988). Whether the molecular mechanisms altered in ASDs are associated with the development of specific human cortical circuits, including minicolumns, remains unknown.

Here, we report that FMRP binds human neuronal *nitric oxide synthase 1* (*NOS1*, also known as *nNOS*) mRNA and increases its translation in the developing neocortex in a species-dependent manner. NOS1 produces the gaseous signaling molecule nitric oxide (NO), which plays important roles in the development and function of the nervous system (Bredt and Snyder, 1994; Garthwaite, 2008). Our study of *NOS1* posttranscriptional regulation was instigated by our observation of a marked discrepancy between the midfetal human neocortex expression patterns of *NOS1* mRNA, which is widespread, and NOS1 protein, which is restricted to layer- and region-specific subpopulations of pyramidal neurons. These include layer 5 (L5) subcortically-projecting neurons with an alternating minicolumnar arrangement in the frontoparietal operculum (FOp). The FOp encompasses the prospective Broca's area and orofacial motor cortex, regions involved in speech production and language comprehension (Keller et al., 2009). After our screen for RNA-binding proteins revealed that FMRP is abundantly bound to human *NOS1* mRNA, we found that FMRP interacts with sequences in the *NOS1*-coding region that contain G-quartet (GQ) motifs and leads to increased NOS1 protein expression. These motifs are absent from mouse *Nos1* mRNA, and replacing the GQ-containing region of human *NOS1* with the mouse orthologous sequence abrogates FMRP-dependent activation of translation. Concordantly, neocortical NOS1 protein levels are dramatically reduced in human FXS, but not *Fmr1*-deficient mice. Thus, we identified a species-dependent posttranscriptional regulation of human *NOS1* by FMRP in specific neocortical circuits during column development and synaptogenesis, and showed it to be altered in FXS.

RESULTS

NOS1 Protein Is Transiently Expressed in Developing Human Pyramidal Neurons

The current research stems from our unexpected observation that strong NADPH-diaphorase (NADPH-d) activity, a reliable histoenzymatic marker of NOS (Dawson et al., 1991; Hope et al., 1991), is transiently present in subpopulations of pyramidal neurons in the developing human neocortex (Sestan and Kostović, 1994), in addition to its previously reported localization to interneurons and cortical plate (CP) neuropil (Fertuzinhos et al., 2009; Judas et al., 1999). Our comprehensive analysis of pre- and postnatal postmortem brains ranging from 8 postconceptional weeks (PCW) to adulthood identified transient expression of NOS1/NADPH-d in two layer- and region-specific populations of pyramidal neurons with a predominant localization to somata and apical dendrites (Figures 1A–1C; see Figure S1A available online). Specifically, morphologically immature pyramidal neurons expressing NOS1 were present in the middle of the CP corresponding to the future L5 exclusively in the ventrolateral frontal cortex of the FOp and the dorsal part of the anterior insula starting around 15 PCW. One week later, $NOS1^+$ pyramidal neurons were also found in the anterior cingulate cortex (ACC) and adjacent dorsolateral frontoparietal cortex in the upper CP corresponding to the future L2 and L3. NOS1 expression in both of these regions was also temporally regulated. The ACC L2/L3 expression of NOS1 was maintained at high levels throughout the late fetal ages, and decreased during early infancy (Figures 1B and S1A; data not shown). In contrast, L5 expression of NOS1 occurred in two waves. First, the L5 expression was restricted to the FOp, and started at 15 PCW, peaked at 18–20 PCW, and was rapidly downregulated at approximately 23 PCW, after which a small number of $NOS1^+$ pyramidal neurons were present in the ventral part of the anterior insula. Second, sparse pyramidal NOS1 expression was present throughout neocortical L5 in the weeks immediately prior to birth and was progressively downregulated after birth (Figures 1B and S1A; data not shown). Thus, in developing pyramidal neurons, NOS1 expression is precisely regulated, exhibiting temporal, laminar, and regional specificity.

Fetal L5 $NOS1^+$ Pyramidal Neurons Form Alternating Columns

Further analysis of the midfetal FOp L5 $NOS1^+$ pyramidal neurons revealed that they were arranged vertically into alternating arrays of intensely ($NOS1^+$) and lightly ($NOS1^-$) stained pyramidal neurons (Figures 1A and 1C) resembling previously described ontogenetic columns (Rakic, 1988). In contrast the ACC L2/L3 $NOS1^+$ pyramidal neurons were more densely distributed (Figure 1D; FOp L5, 67.86 ± 5.66 cells per 1,000 μm^2; ACC L3, 178.57 ± 27.95 cells per 1,000 μm^2; $p = 4.12 \times 10^{-5}$) and lacked this alternating columnar arrangement (Figure 1E; nearest neighbor distance between cell clusters: FOp L5, 27.87 ± 5.26 μm; ACC L3, 15.75 ± 4.68 μm; $p = 4.24 \times 10^{-9}$). In contrast to midgestation, perinatal $NOS1^+$ L5 neurons did not exhibit columnar organization (Figure S1A).

Because the FOp is structurally and functionally lateralized (Keller et al., 2009), we investigated whether L5 $NOS1^+$ columns exhibited left-right asymmetry in two whole midfetal brains (18 and 20 PCW). Serial reconstruction confirmed the two separate domains of $NOS1^+$ pyramidal neurons in the FOp and ACC of both hemispheres (Figures 1F and S1B) and provided approximate total numbers of FOp $NOS1^+$ columns (18 PCW: 41,380; and 20 PCW: 45,150). Although the number of $NOS1^+$ columns was not significantly different between the left and right hemispheres ($p = 0.569$), the distribution of $NOS1^+$ columns showed an asymmetric trend, peaking more rostrally in the right hemisphere, in both brains. Thus, the columnar organization of $NOS1^+$ neurons in the midfetal FOp L5 is bilaterally present.

Molecular and Projectional Identity of $NOS1^+$ Pyramidal Neurons

To molecularly characterize the identity of $NOS1^+$ neurons, we examined their expression of neuronal subtype markers. In the midfetal FOp L5, markers of subcortically-projecting pyramidal neurons, BCL11B (CTIP2) and *FEZF2* (*FEZL*, *ZFP312*) (Chen et al., 2005; Kwan et al., 2008; Leone et al., 2008; Molyneaux et al., 2007), were selectively coexpressed by L5 $NOS1^+$

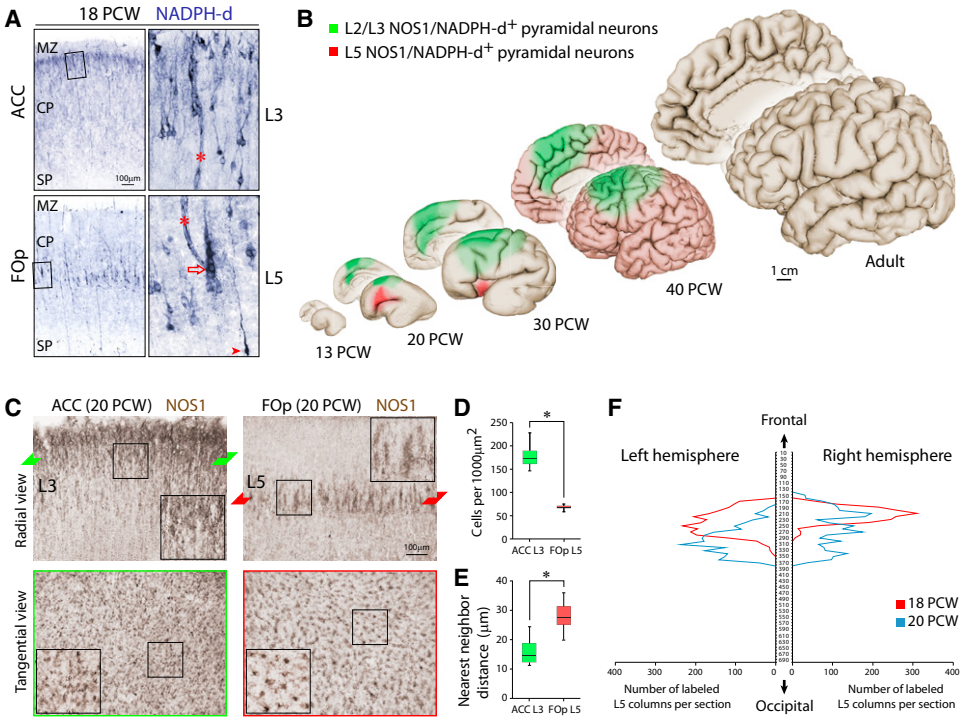

Figure 1. Spatiotemporal Dynamics of NOS1 Expression in Pyramidal Neurons of the Human Neocortex

(A) NADPH-d histochemistry at 18 PCW revealed intensely labeled pyramidal neurons in ACC L3 and FOp L5, where stained neurons were arranged into alternating vertical columns (open arrow). Interneurons (arrowhead) and blood vessels (asterisks) were also labeled. Boxes represent the 25th, 50th, and 75th percentiles.

(B) Schematic summary of the spatiotemporal dynamics of NOS1/NADPH-d staining in pyramidal neurons of L2/L3 (green) and L5 (red) in the developing and adult human neocortex.

(C) NOS1 immunohistochemistry of radial and tangential sections at 20 PCW. NOS1$^+$ pyramidal neurons exhibited a clear columnar organization in FOp L5, but not ACC L3.

(D and E) Analysis of cell density (D) and cluster spacing (E) revealed that NOS1$^+$ neurons in FOp L5 were significantly distinct in cytoarchitectonic organization from those in ACC L3. *$p < 0.05$. Boxes represent the 25th, 50th, and 75th percentiles. Error bars represent the 5th and 95th percentiles of 30 measurements.

(F) Serial section analysis of NADPH-d$^+$ L5 columns in two brains at 18 and 20 PCW. NADPH-d$^+$ columns were present bilaterally.

See also Figure S1.

neurons, forming an alternating columnar pattern identical to that of NOS1 (Figures 2A, 2B, and 2D). NOS1$^+$ neurons also coexpressed *FOXP2* (Figure 2E), a gene altered in a developmental disorder characterized by impaired speech and linguistic deficits (Lai et al., 2001). In contrast, SATB2, a marker of upper-layer corticocortical pyramidal neurons (Britanova et al., 2008), was highly expressed in NOS1$^-$, but not NOS1$^+$, neurons (Figures 2A and 2B), suggesting that NOS1$^-$ neurons were later born and likely migrating in between L5 NOS1$^+$ columns to the upper layers. Consistent with this, we observed vimentin (VIM)-positive radial glial fibers in between but not within NOS1$^+$ columns (Figure S2A). This suggests that glial-guided migration of upper-layer neurons occurs via corridors formed between L5 neuronal columns. In the ACC, all L2/L3 NOS1$^+$ neurons coexpressed SATB2 (Figure S2B), confirming their upper-layer identity and distinction from the FOp L5 NOS1$^+$ neurons.

To examine whether the midfetal pyramidal neurons of diverse subtypes have distinct cytoarchitectonic arrangements, we first measured the nearest neighbor ratio (NNR) and total path length ratio (TPLR) (Buxhoeveden et al., 1996) of NOS1$^+$ and NOS1$^-$ L5 neurons in the 20 PCW FOp (Figure 2C). This confirmed that NOS1$^+$ L5 neurons were significantly closer to being perfectly columnar (1.0) compared to NOS1$^-$ L5 neurons, as determined by both NNR (NOS1$^+$, 1.145 ± 0.146; NOS1$^-$, 1.528 ± 0.202; $p = 2.97 \times 10^{-5}$) and TPLR (NOS1$^+$, 1.122 ± 0.077; NOS1$^-$, 1.740 ± 0.369; $p = 2.41 \times 10^{-3}$). Next, we retrogradely traced projection neurons in a postmortem 20 PCW brain. We labeled subcortical projection neurons with Fast DiI inserted into the internal capsule and corticocortical projection neurons with Fast DiA inserted into the corpus callosum (Figure 2H). DiI-labeled subcortical projection neurons in the FOp formed columns similar in organization to the NOS1$^+$ columns (Figure 2I). In contrast, DiA-labeled callosal neurons in the ACC did not exhibit columnar organization (Figure 2J). Collectively, these results indicate that FOp NOS1$^+$ neurons exhibit the columnar organization and molecular identity of postmigratory L5 subcortically-projecting neurons.

Transient NOS1 Expression in Pyramidal Neurons Is Concomitant with Early Synaptogenesis

Previous studies have shown that significant neocortical synaptogenesis starts during midgestation (Molliver et al., 1973).

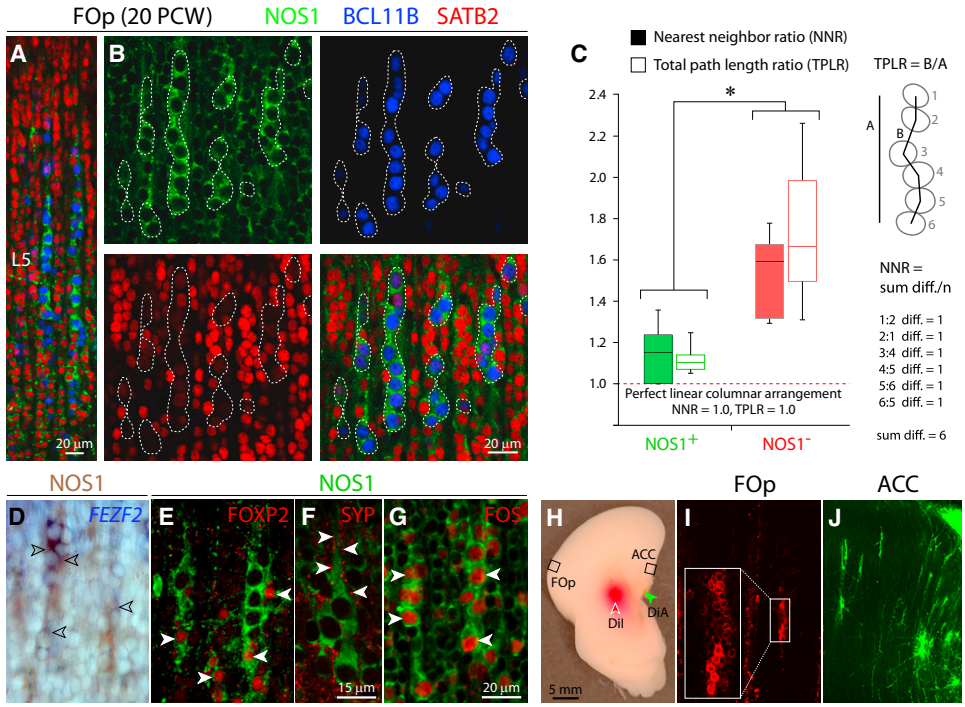

Figure 2. Molecular, Structural, and Axonal Connectivity Analyses of L5 NOS1$^+$ Columns in the Midfetal Human FOp

(A and B) Triple-immunofluorescent staining for NOS1 (green), BCL11B (blue), a marker of L5 subcortically-projecting neurons, and SATB2 (red), a marker of upper-layer corticocortical projection neurons, in 20 PCW FOp L5. NOS1$^+$ and BCL11B$^+$ pyramidal neurons formed alternating columns (outlined) separated by clusters of SATB2$^+$ neurons.

(C) Analysis of columnarity in FOp L5 neurons. NOS1$^+$ neurons were significantly more columnar in organization compared to NOS1$^-$ neurons. *$p < 0.05$. Boxes represent the 25th, 50th, and 75th percentiles. Error bars represent the 5th and 95th percentiles of 30 measurements. diff, difference.

(D) NOS1 immunostaining (brown) and *FEZF2* in situ hybridization (blue) of FOp L5 at 18 PCW. NOS1$^+$ neurons coexpressed *FEZF2* (open arrowheads).

(E–G) Immunofluorescent staining for NOS1 (green) and FOXP2, SYP, or FOS (red in E–G). NOS1$^+$ neurons coexpressed FOXP2 and FOS (arrowheads in E and G) and were encircled by SYP puncta (arrowheads in F).

(H–J) Retrograde axonal tracing at 20 PCW. Retrograde travel of Fast DiI inserted into dorsal internal capsule (red arrowhead) and Fast DiA inserted into the corpus callosum (green arrowhead) were examined after 7 months in incubation. In the FOp L5 (I), DiI-labeled subcortical projection neurons formed columns similar to those composed of NOS1$^+$ neurons. In the ACC (J), DiA-labeled corticocortical projection neurons did not exhibit obvious columnar organization. White box in (I) represents area enlarged in inset.

See also Figure S2.

Consistent with the possibility that NOS1 expression is associated with synaptogenesis, we found presynaptic synaptophysin (SYP) puncta encircling the cell membrane of FOp NOS1$^+$ L5 neurons at the soma and apical dendrite (Figure 2F). Our pre-embedding NOS1 immuno-EM in the 18 and 20 PCW FOp, however, revealed only sparse mature synapses in the CP (Figures S2C and S2D), suggesting that the majority of SYP$^+$ puncta on L5 NOS1$^+$ columns were immature terminals. Concordantly, immature synapses that have not yet become electron dense or accumulated vesicles and nonsynaptic contacts were observed in L5 and on NOS1$^+$ dendrites (Figures S2E–S2H). Interestingly, FOS (C-FOS), a marker of recent neuronal activity, was expressed by virtually all NOS1$^+$ columnar neurons and was mostly absent from NOS1$^-$ intercolumnar neurons in the 20 PCW FOp (Figure 2G), suggesting that NOS1$^+$ L5 neurons may be active. Together, these findings suggest that the expression of NOS1 in L5 FOp neurons is concomitant with early synaptogenesis and neuronal activity.

Cross-Species Comparison of Neocortical NOS1 Expression

To determine whether the spatiotemporal expression pattern of NOS1 exhibits species differences, we examined NADPH-d/NOS1 expression in the gyrated macaque monkey neocortex and lissencephalic mouse neocortex (Figure 3; data not shown). In the macaque, NADPH-d$^+$ pyramidal neurons were present in L2/L3 of the ACC and adjacent frontoparietal regions, starting as early as embryonic day (E) 62, an age equivalent to human midgestation (Kostovic and Rakic, 1990), and persisting until the late fetal period (Figures 3B and S3; data not shown). NADPH-d$^+$ pyramidal neurons were present in L5 columns of the FOp and adjacent regions (Figures 3B and 3C), starting as early as E73, peaking near E82, and persisting until at least E113 (Figures 3B and S3; data not shown). Consistent with previous studies, our analyses of the mouse neocortex from E18.5 to P14, a period equivalent to human midfetal to early postnatal development, revealed that intense NADPH-d activity was present exclusively in interneurons and neuropil (Figure 3A;

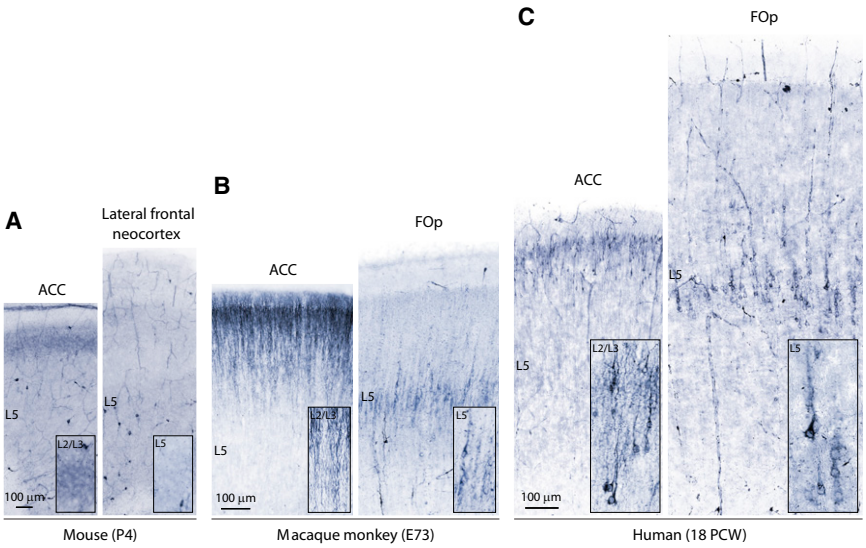

Figure 3. Comparative Analysis of NADPH-d Activity in Mouse, Macaque, and Human Neocortex at Equivalent Developmental Ages

In the P4 mouse ACC and lateral frontal cortex (A), intense NADPH-d staining was restricted to interneurons, with neuropil staining in ACC L2/L3. In the E73 macaque neocortex (B), intense NADPH-d activity was present in ACC L2/L3 pyramidal neurons similar to those labeled in the human 18 PCW ACC (C). In the macaque FOp, NADPH-d$^+$ L5 pyramidal neurons were arranged into vertical columns similar in organization to the human FOp columns (C). Strong interneuronal and weak neuropil NADPH-d staining was present in all cortical areas in mouse, macaque, and human neocortex. See also Figure S3.

data not shown), indicating that pyramidal expression of NOS1 is species dependent.

Discordant *NOS1* mRNA and Protein Expression Patterns in the Fetal Neocortex

To examine the expression pattern of *NOS1* mRNA, adjacent tissue sections of the midfetal neocortex were analyzed with *NOS1* in situ hybridization, NADPH-d, and NOS1 immunostaining (Figure 4A). Surprisingly, *NOS1* mRNA was abundantly and widely present in the CP in all cortical layers and regions examined, including the great majority of pyramidal neurons that did not express NOS1 protein. This striking difference between the highly restricted NOS1 protein and widespread *NOS1* mRNA expression suggests that *NOS1* is posttranscriptionally regulated.

Remarkably, *Nos1* mRNA was also abundantly and widely expressed in the early postnatal mouse neocortex (Figure 4B). Pyramidal expression of mouse *Nos1* mRNA was confirmed by quantitative RT-PCR of fluorescently sorted pyramidal neurons fate mapped in mice doubly transgenic for *Emx1-Cre* and a CRE-responsive *Gfp* (*CAG-Cat-Gfp*) (Figure 4C). Therefore, whereas *NOS1* mRNA is expressed in pyramidal neurons of both human and mouse neocortex, its efficient translation into NOS1 protein occurs in subpopulations of human, but not mouse, pyramidal neurons. This indicates that pyramidal NOS1 expression is driven by species-dependent posttranscriptional regulation.

NOS1 mRNA Associates with FMRP in Human Fetal Neocortex

To identify potential *NOS1* mRNA-binding proteins, we used immobilized full-length human *NOS1* mRNA to pull down candidate proteins from the human frontal CP at 20 and 21 PCW. To facilitate the isolation of sequence-dependent RNA-binding proteins, we used three negative control RNAs (*GAPDH*, *EGFP*, and *NeoR*). *NOS1* mRNA-interacting proteins showed a distinct enrichment at a molecular weight of approximately 75 kDa (Figure 5A). To identify the protein present in this band, we analyzed our human brain transcriptome data set (http://www.humanbraintranscriptome.org; Johnson et al., 2009; Kang et al., 2011) for RNA-binding proteins near 75 kDa that are expressed in the midfetal frontal neocortex. Analysis of four candidates (FMRP, FXR1, CPEB3, and EIF2C2) by immunoblotting of pulled-down proteins revealed that FMRP, but not the others, was strongly and specifically associated with *NOS1* mRNA (Figures 5A and S4A). The presence of FMRP in this *NOS1*-enriched band was confirmed by mass spectrometry (data not shown), which also revealed the putative presence of PABPC4, a poly-adenylate-binding protein, and HSPA8, a chaperone protein. Double-immunofluorescent staining showed that FMRP was highly coexpressed in NOS1$^+$ pyramidal neurons in the midfetal FOp and ACC (Figures 5B and S4B). Subcellularly, FMRP and NOS1 colocalized to the soma and apical dendrite. Interestingly, most NOS1$^+$ interneurons in the SP and CP did not express FMRP at high levels during midgestation. Together, these results suggest a potential role of FMRP in the posttranscriptional regulation of *NOS1* in fetal human pyramidal neurons.

Species Differences in FMRP-*NOS1* mRNA Association in the Developing Neocortex

To confirm the putative FMRP-*NOS1* mRNA interaction, we performed RNA-binding protein immunoprecipitation (RIP) using 21 PCW frontal CP lysate. RNAs coimmunoprecipitated with FMRP were analyzed using quantitative RT-PCR (Figure 5C). Compared to rabbit immunoglobulin (IgG) control, anti-FMRP antibodies immunoprecipitated 6.8- ± 0.8-fold more *NOS1* mRNA, a level of enrichment similar to *MAP1B* mRNA (7.1- ± 0.6-fold), a well known target of FMRP (Darnell et al., 2011), and significantly higher than *GAPDH* mRNA (1.5- ± 0.4-fold), a negative control. In contrast in the early postnatal mouse neocortex (Figure 5D), *Nos1* mRNA was enriched only 2.7- ± 0.3-fold by anti-FMRP immunoprecipitation, markedly lower than the 8.6- ± 0.5-fold enrichment for *Map1b* mRNA and comparable to *Gapdh* mRNA (2.0- ± 0.1-fold). Consistent with

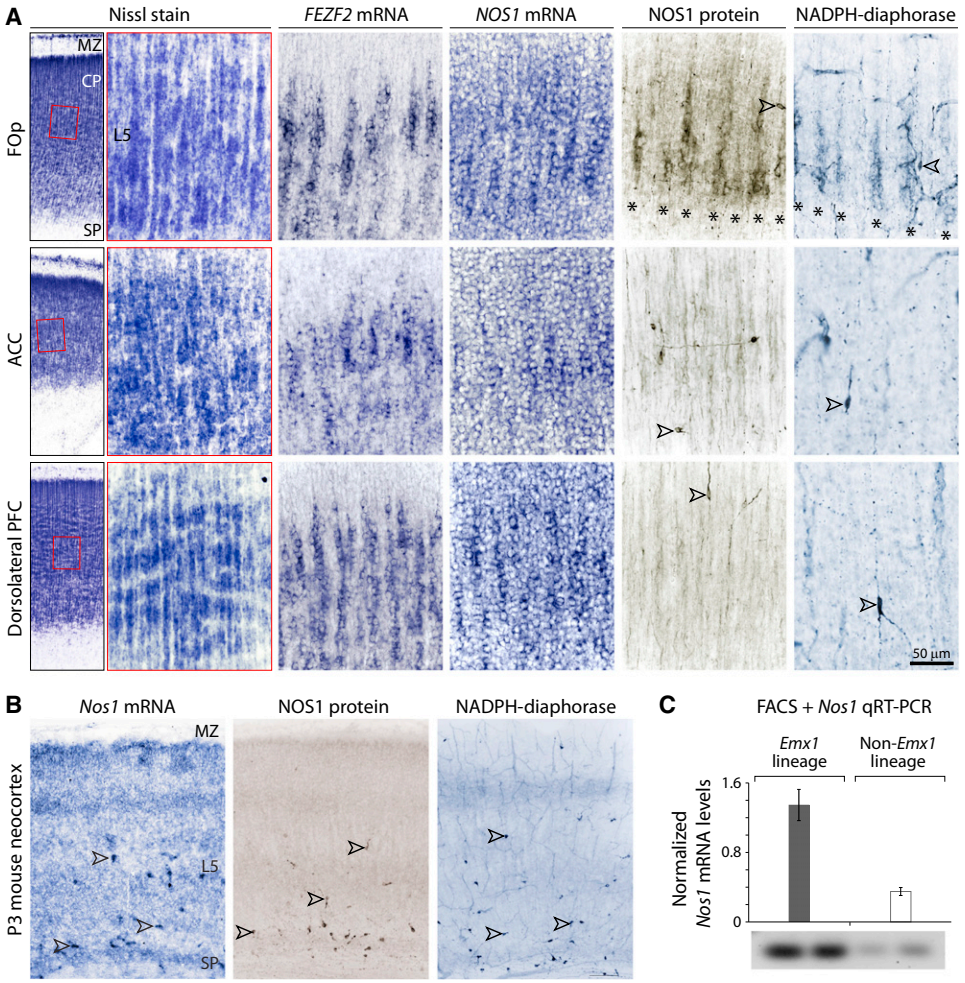

Figure 4. Discordant *NOS1* mRNA and NOS1 Protein Expression Patterns in the Developing Human and Mouse Neocortex

(A) Nissl staining, *FEZF2* and *NOS1* in situ hybridization, NOS1 immunohistochemistry, and NADPH-d histochemistry in adjacent sections from 18 PCW FOp, ACC, and dorsal lateral prefrontal cortex (PFC). *NOS1* mRNA was abundantly present in all cortical regions and layers examined. Intense NOS1 and NADPH-d labeling in L5 pyramidal columns (asterisks) were present in the FOp. In all examined cortical regions, NOS1 and NADPH-d were present in interneurons (open arrowheads) and neuropil. Red boxes represent areas enlarged.

(B) *Nos1* in situ hybridization, NOS1, and NADPH-d staining in adjacent sections from P3 mouse frontal neocortex. *Nos1* mRNA was widely present; intense NOS1 and NADPH-d stainings were exclusively present in interneurons (open arrowheads). Neuropil was weakly stained. MZ, marginal zone; SP, subplate.

(C) Pyramidal neurons of the *Emx1* lineage were isolated from the P3 mouse neocortex by fluorescent cell sorting (FACS) and analyzed by quantitative (q) RT-PCR. *Nos1* mRNA was abundantly present in pyramidal neurons. Error bars represent the 5th and 95th percentiles of four measurements.

this, *Nos1* was absent from the FMRP targets identified in a recent, comprehensive HITS-CLIP analysis of the mouse brain (Darnell et al., 2011). Thus, FMRP strongly associates with human but not mouse *NOS1* mRNA in the developing neocortex, suggesting that FMRP may underlie species differences in *NOS1* translation.

FMRP Binds GQ-Containing Sequences in the Human *NOS1*-Coding Region

FMRP can interact with specific mRNA sequences including GQ structures (Darnell et al., 2001; Schaeffer et al., 2001) and poly-uridine stretches (Chen et al., 2003). Analysis of human *NOS1* mRNA revealed three putative GQ motifs and six poly-uridine stretches (Figure 6A). RNA pull-down assays from 21 PCW frontal CP lysate revealed that FMRP had strong affinity for each of the two *NOS1*-coding region GQs (GQ1 and GQ2), but not GQ3 or the U-rich regions (UR1–UR6) (Figure 6B). To confirm this, we synthesized a fragment of RNA representing both GQ1 and GQ2 and performed an electrophoretic mobility shift assay (EMSA; Figure 6C). In the presence of FMRP, this RNA exhibited a significant shift that was abolished by the addition of excess nonbiotinylated "cold" RNA or a neutralizing FMRP antibody. To determine whether human GQ1 and GQ2 form RNA G-quadruplex structures, we used a reverse-transcription termination assay (Figure 6D). Reverse-transcriptase activity pauses at sites of GQ structures in a cation-dependent manner (Schaeffer et al., 2001). Reverse transcription from both GQ1 and GQ2 RNA exhibited a significant pause at the expected GQ site in the

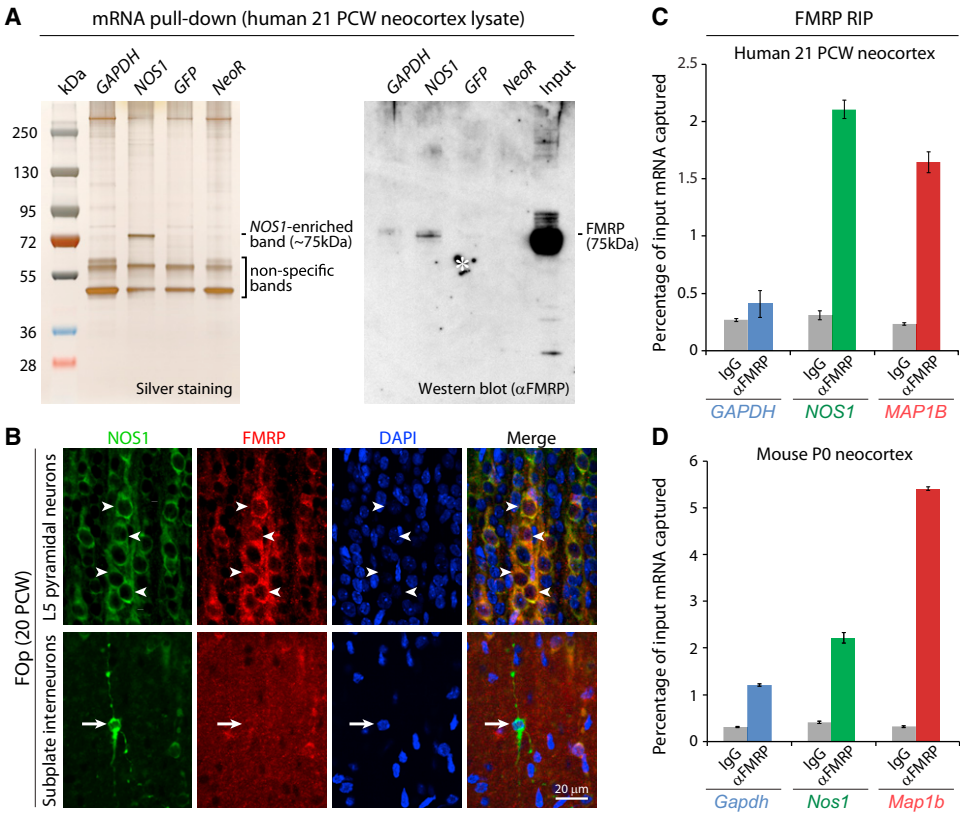

Figure 5. FMRP Binds *NOS1* mRNA in the Human Fetal Neocortex

(A) Proteins eluted from an mRNA pull-down assay using lysates of a 21 PCW human neocortex were analyzed by silver staining and immunoblotting. *NOS1*, but not control (*GAPDH*, *GFP*, and *NeoR*), mRNA specifically associated with an ~75 kDa protein that was immunopositive for FMRP. Asterisk indicates an artifact of gel transfer.

(B) NOS1 (green), FMRP (red), and DAPI (blue) staining of 20 PCW FOp. FMRP was coexpressed by L5 columnar NOS1$^+$ pyramidal neurons (solid arrowheads), but not most interneurons (arrows).

(C and D) FMRP immunoprecipitated mRNAs from a 21 PCW human and P0 mouse CP were analyzed by quantitative RT-PCR. Relative to control *GAPDH* and *MAP1B* mRNAs, FMRP strongly associated with *NOS1* mRNA (green bar) in human, but not mouse. Error bars represent the 5th and 95th percentiles of four measurements.

See also Figure S4.

presence of potassium, which facilitates GQ formation, but not lithium, which abrogates it. Therefore, FMRP interacts with GQ-forming sequences found within the coding region of human *NOS1* mRNA.

Evolution of *NOS1* mRNA GQ-Containing Sequences

To investigate whether GQ motifs are present in other mammals, we analyzed the 21 species for which *NOS1* mRNA sequence was available. Highly stable tetrads at both GQ1 and GQ2 positions were predicted only in the great apes and macaque monkey (Figure S5A). Among great apes, which otherwise have perfectly conserved GQs, only orangutan has a point mutation that leads to a less stable two-stack GQ1 quartet, but a fully conserved GQ2 quartet. In marmoset, a New World monkey, and nonprimate mammals, with the exception of the guinea pig that exhibited one quartet, they are absent from both positions. Further analysis of the entire *NOS1* coding region in nine placental mammals revealed a very high degree of conservation (Figure S5B), with the vast majority of substitutions being synonymous. The few nonsynonymous substitutions, however, were selectively clustered in the GQ region. This marked reduction in amino acid identity in an otherwise highly conserved protein is consistent with the hypothesis that the sequences containing the GQ motifs evolved and made possible posttranscriptional regulation by FMRP. Furthermore, these sequences have remained quite stable since their emergence in catarrhine primates, which is consistent with the expression of NOS1 in human and macaque pyramidal neurons.

FMRP Increases NOS1 Expression via Interaction with a GQ-Containing Sequence

To test the functional consequences of FMRP on *NOS1* translation, we cotransfected human expression constructs of FMRP (CAG-h*FMR1*) and NOS1 (CAG-h*NOS1*) into Neuro-2a cells and quantified NOS activity (Figure 6E). With CAG-h*FMR1* cotransfection, NOS1 activity was increased in a dose-dependent manner, by up to 3.6- ± 0.9-fold ($p = 0.043$), indicating that

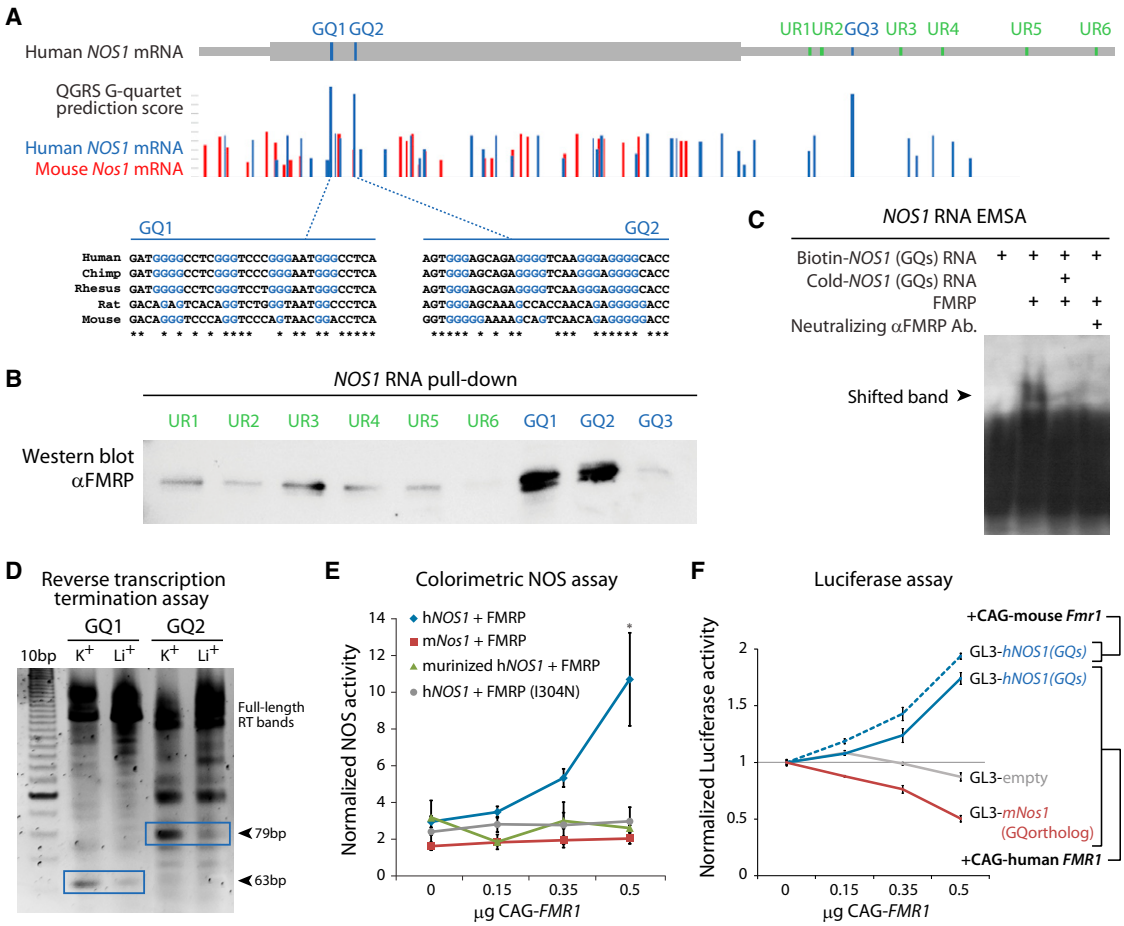

Figure 6. FMRP Binds Human *NOS1* GQ-Containing Sequences and Enhances Human, but Not Mouse, *NOS1* mRNA Translation

(A) Prediction of putative FMRP-binding GQ and U-rich (UR) motifs in the human *NOS1* mRNA sequence and alignment of GQ1 and GQ2. GQ1 and GQ2 were highly conserved in primates, but not rodents.

(B) FMRP association with each putative binding motif was analyzed by an mRNA pull-down assay using 21 PCW human neocortex lysates. FMRP selectively associated with GQ1 and GQ2.

(C) EMSA of GQ1 and GQ2. RNA containing both GQs exhibited a significant shift in mobility in the presence of FMRP. This shift was abolished by addition of excess unbiotinylated ("cold") RNA or a neutralizing anti-FMRP antibody.

(D) Reverse-transcription termination assay. Reverse transcription paused at the expected GQ sites for both GQ1 and GQ2 in the presence of K^+, which facilitates GQ formation, but not Li^+, which disrupts it.

(E) Colorimetric NOS assays in Neuro-2a cells cotransfected with CAG-h*FMR1* or CAG-h*FMR1*(I304N) and one of CAG-h*NOS1*, CAG-m*Nos1*, or CAG-murinized-h*NOS1*. NOS activity from h*NOS1*, but not m*Nos1* or murinized h*NOS1*, increased dose dependently with increasing wild-type FMRP. The I304N mutation in FMRP abolished its activation of h*NOS1* translation. *$p < 0.05$. Error bars represent the 5th and 95th percentiles of four measurements.

(F) Luciferase assays in Neuro-2a cells transfected with an empty reporter construct (GL3-empty), or constructs containing the human *NOS1* GQs (GL3-h*NOS1*[GQs]) or the orthologous sequence in mouse *Nos1* (GL3-m*NOS1*[GQortholog]). Luciferase activity in cells transfected with GL3-h*NOS1*(GQs) increased dose dependently with cotransfection of human CAG-h*FMR1* (solid blue line) or mouse CAG-m*Fmr1* (broken blue line). Luciferase activity from the GL3-m*Nos1* (GQortholog) decreased with increasing amounts of CAG-h*FMR1* (solid red line). Error bars represent the 5th and 95th percentiles of six measurements.

See also Figure S5.

FMRP acts as a positive regulator of NOS1 expression. No increase in NOS1 activity occurred when a mouse *Nos1* construct (CAG-m*Nos1*) or a human *FMR1* construct harboring the I304N mutation (CAG-h*FMR1* [I304N]) (Siomi et al., 1994) was used, or when the GQ-containing sequence of the human *NOS1* was replaced with the orthologous sequence from mouse *Nos1* (CAG-murinized-h*NOS1*). Therefore, the FMRP-mediated increase in NOS1 expression is dependent on the species of the *NOS1* sequence, the intact KH2 domain of FMRP, and the presence of GQ-containing sequences in the *NOS1* mRNA. To specifically examine the GQ region, we cloned the *NOS1* sequences containing GQ1 and GQ2 into the 3′ UTR of SV40-GL3 and performed luciferase assays in Neuro-2a cells (Figure 6F). The inclusion of the human *NOS1* GQs (SV40-GL3-h*NOS1*-GQs) led to significant dose-dependent increases in luciferase activity in response to CAG-h*FMR1*, indicating that FMRP increases *NOS1* translation via binding to these sequences. Importantly, a mouse FMRP expression construct

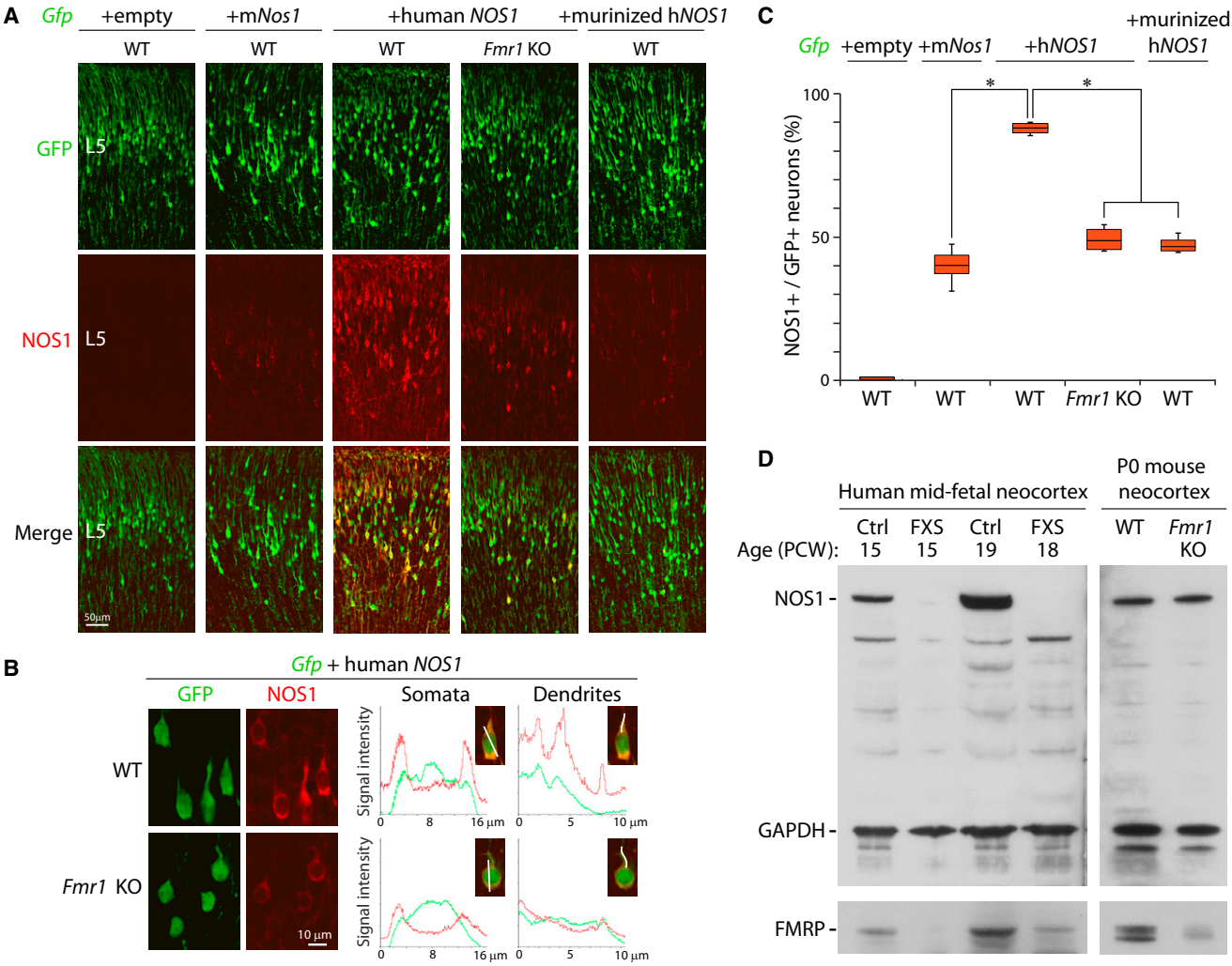

Figure 7. Efficient Translation of Human *NOS1* in Pyramidal Neurons Requires FMRP and Is Severely Reduced in Fetal FXS Neocortex

(A–C) Neocortex of wild-type or *Fmr1* KO mouse electroporated in utero at E13.5 and immunostained for NOS1 (red) at P0. In wild-type neocortex the majority of pyramidal neurons transfected with h*NOS1* expressed high levels of NOS1 properly localized to the soma and apical dendrite. NOS1 protein expression from m*Nos1* or murinized-h*NOS1* in wild-type and from h*NOS1* in *Fmr1* KO neocortex was dramatically reduced in comparison. The fluorescent intensity of NOS1 staining normalized to GFP (B) and the proportion of GFP^+ cells expressing NOS1 (C) were quantified. *$p < 0.05$. Boxes represent the 25^{th}, 50^{th}, and 75^{th} percentiles. Error bars represent the 5^{th} and 95^{th} percentiles of at least four animals.

(D) Immunoblots of human fetal FXS and P0 mouse *Fmr1* KO neocortex. Normalized to *GAPDH* levels, the neocortical expression of NOS1 protein was severely reduced in both human fetal FXS cases. In neonatal mouse neocortex, loss of *Fmr1* did not alter neocortical NOS1 expression.

See also Figure S6.

(CAG-m*Fmr1*) dose dependently increased luciferase expression in a manner highly similar to CAG-h*FMR1*. However, when the human *NOS1* GQ sequences were replaced with the orthologous region of the mouse *Nos1* (SV40-GL3-m*Nos1*-GQortholog), FMRP failed to enhance luciferase activity. These results indicate that FMRP activates NOS1 protein expression via binding to a sequence containing GQ motifs and that this interaction exhibits species differences. Together, these data strongly support a scenario wherein FMRP activation of *NOS1* translation evolved through *NOS1* nucleotide substitutions that gave rise to a GQ-containing sequence targeted by FMRP.

Mouse Pyramidal Neurons Efficiently Translate Human NOS1 in an FMRP-Dependent Manner

Because mouse FMRP is able to enhance human NOS1 expression, we hypothesized that exogenous human *NOS1* mRNA can be efficiently translated in mouse pyramidal neurons, likely in an *Fmr1*-dependent manner. To test this in vivo, we introduced a *NOS1* expression construct with the CAG-*Gfp* reporter into mouse neocortical ventricular zone (VZ) using in utero electroporation (IUE) at E13.5 to target L5 pyramidal neurons. At P0, the majority of CAG-h*NOS1*-electroporated L5 pyramidal neurons expressed NOS1 protein at high levels (Figures 7A–7C). In contrast those electroporated with CAG-m*Nos1* or

CAG-murinized-h*NOS1* expressed only low levels of NOS1 in a minority of neurons, indicating reduced protein expression efficiency consistent with our in vitro assays. Human and mouse NOS1 exhibited similar somatodendritic localization (Figures 7A and 7B). Therefore, our results show that mouse pyramidal neurons possess all of the cellular machinery necessary for the translation of human NOS1 protein and suggest that their diminished expression of endogenous NOS1 is a result of differences in the *NOS1* mRNA sequence between human and mouse.

To assess FMRP dependence, we further electroporated *Fmr1* knockout (KO) mice with CAG-h*NOS1* and CAG-*Gfp* (Figure 7A). Both the number of GFP^+ neurons expressing NOS1 and the levels of NOS1 protein decreased significantly compared to wild-type (Figures 7B and 7C). In addition, neurons cultured from E14.5 *Fmr1* KO and transfected with CAG-h*NOS1* also exhibited a significant reduction in NOS1 levels compared to control (Figure S6A; 43.8% ± 7.8% reduction; $p = 0.0065$). These data show that FMRP is required for the efficient expression of human NOS1 protein in pyramidal neurons.

Severe Reduction in NOS1 Protein Levels in Developing Human FXS but Not Mouse *Fmr1* KO Neocortex

To determine whether NOS1 protein levels are altered in human FXS cases, we performed immunoblotting of neocortex from confirmed midfetal and postnatal FXS cases (15 and 18 PCW; and 9, 22, and 85 years) and age-matched controls. Neocortical lysates normalized to *GAPDH* levels were immunoblotted for NOS1, FMRP, and GAPDH (Figure 7D). Remarkably, in both fetal cases of FXS, neocortical NOS1 protein levels were severely reduced compared to matched controls. Furthermore, this deficit was age dependent, being very dramatic in the fetal cases, less so in the cases aged 9 and 22 years, and absent in the 85 years' specimen (Figure S6C). These results indicate that NOS1 protein expression is greatly reduced in the developing human FXS neocortex. Notably, neocortical NOS1 levels were not affected in early postnatal *Fmr1* KO mice (Figures 7D and S6B), indicating that the requirement of FMRP for NOS1 expression is species dependent.

DISCUSSION

In this study we demonstrate that human neocortical NOS1 expression is posttranscriptionally regulated by FMRP in a species-dependent manner. Molecular analyses revealed that FMRP binds GQ motif-containing sequences present in the coding region of human, but not mouse, *NOS1* mRNA and facilitates NOS1 protein expression. Concordantly, NOS1 expression is severely reduced in the developing FXS human, but not FMRP-deficient mouse, neocortex. In the human neocortex, NOS1 and FMRP are transiently coexpressed during synaptogenesis in subpopulations of pyramidal neurons in regions involved in speech, language, and complex social behaviors. Together, these findings provide a novel candidate mechanism and insights into the potential connectional pathology of FXS and possibly ASD.

Our analyses indicate that the FMRP-*NOS1* interaction emerged as result of closely clustered nucleotide substitutions within the otherwise highly conserved coding sequence of *NOS1* that gave rise to the GQ-containing motifs, occurring at the potential expense of protein integrity. FMRP binding to GQ motifs has been associated with translational repression (Bechara et al., 2009; Schaeffer et al., 2001). There is, however, a precedent for positive, activity-dependent posttranscriptional regulation in *PSD-95* (*DLG4*), which has an FMRP-binding GQ motif (Todd et al., 2003; Zalfa et al., 2007). Interestingly, NOS1 and PSD-95 are functionally related. NOS1 is anchored to the synaptic membrane via a physical interaction with PSD-95 (Brenman et al., 1996) and its enzymatic product, NO, *S*-nitrosylates PSD-95 (Ho et al., 2011). Although the abundant presence of *NOS1* mRNA in pyramidal neurons suggests that translational regulation is involved, FMRP may also control the stability of the *NOS1* transcript in a manner similar to its control of *PSD-95* mRNA stability (Zalfa et al., 2007). Furthermore, the GQ motif has been shown to mediate the dendritic localization of *PSD-95* (Dictenberg et al., 2008) and may also play a role in *NOS1* mRNA targeting. The possibility that *NOS1* and *PSD-95* are similarly regulated by FMRP is consistent with their shared postsynaptic localization, physical interaction, and related functions. The binding of FMRP to GQs has been demonstrated both in vitro (Bagni and Greenough, 2005; Bassell and Warren, 2008) and in vivo (Rackham and Brown, 2004; Iioka et al., 2011). Recently, however, it was shown that the presence GQ motifs is not predictive of FMRP binding (Darnell et al., 2011). Therefore, the context dependence of FMRP interactions with GQs remains to be fully elucidated, and individual potential interactions should be validated empirically.

Animal models of FXS exhibit multiple phenotypes present in human FXS, indicating that many aspects of FMRP function are well conserved. Therefore, any contribution of NOS1 to the FXS phenotype would likely involve the higher cognitive functions that are absent from mouse. This possibility is supported by the coexpression of NOS1 and FMRP in projection neurons of the FOp and the ACC and adjacent dorsal frontoparietal neocortex. The FOp encompasses the future Broca's area and its contralateral hemisphere equivalent, as well as the orofacial motor cortex, regions involved in speech production, language comprehension, and action recognition (Keller et al., 2009). The ACC is involved in decision making, attention, emotional processing, and social awareness (Devinsky et al., 1995). NOS1 expression in these regions is also temporally regulated from midgestation to early infancy, a developmental period critical for early synaptogenesis, dendritic spine formation, and ingrowth of cortical afferents (Kang et al., 2011). Therefore, the neuroanatomical localization and timing of the FMRP-*NOS1* interaction are consistent with a putative role in the development of neocortical circuits, including those involved in linguistic and social functions likely affected in FXS and ASD.

This potential role of *NOS1* in the development and function of human neural circuits is further supported by studies of a human *NOS1* hypomorphic allele, which has been associated with attention deficit hyperactivity disorder (ADHD), impulsivity, and aggression (Reif et al., 2009), behavioral features often comorbid with FXS (Rogers et al., 2001). This *NOS1* hypomorphism has also been associated with hypoactivity in the ACC (Reif et al., 2009), a cortical region with prominent midfetal pyramidal

expression of NOS1 protein. Functional imaging studies revealed a similar reduction in ACC activation in patients with FXS and ADHD during attentional-processing tasks (Bush et al., 1999; Menon et al., 2004) and in autistic children in response to a familiar face (Pierce and Redcay, 2008). The overlapping deficits between NOS1 hypomorphism, FXS, and FXS comorbidities are consistent with a functional role of *NOS1* in human brain circuitry related to FXS and ASD. Furthermore, the two midfetal neocortical regions with prominent pyramidal NOS1 expression, the ACC and FOp, exhibit highly coordinated resting state activity, suggesting functional connectivity between the two areas and the presence of a cingulo-opercular cognitive network (Power et al., 2011). Interestingly, the connectivity of this cingulo-opercular network has been reported to be impaired in schizophrenia (Tu et al., 2012). Remarkably, multiple sequence variations in *NOS1* have been associated with schizophrenia (Cui et al., 2010; Reif et al., 2006; Shinkai et al., 2002), supporting a potential role of NOS1 in the formation of cognitive circuits and in disorders that affect cognition.

Structural alteration in the organization of minicolumns has been reported in autism and other psychiatric disorders (Casanova et al., 2002). In this study we found that within the midfetal FOp, alternating L5 columns coexpress FMRP and NOS1, as well as FOXP2, which is implicated in the development of speech, language, and cognition (Lai et al., 2001), functions affected in FXS and ASD. We also showed that neurons within the same column have a shared subcortical molecular identity and connectivity. Positioned in between the columns are migratory corridors containing radial glial fibers and corticocortical projection neurons en route to the superficial layers. Thus, this fetal organization may have implications for the developmental basis of normal minicolumns (Rakic, 1988), as well as columnopathies (Casanova et al., 2002). Interestingly, the $NOS1^+$ columnar neurons of the fetal FOp share some areal and projection properties with adult mirror neurons, which are present in macaque area F5 (Rizzolatti and Craighero, 2004), an area equivalent to the human Broca's area, and project subcortical axons (Kraskov et al., 2009). Mirror neurons, which are activated during both the observation and execution of a particular goal-directed action, are thought to contribute to theory of mind and language abilities (Rizzolatti and Craighero, 2004), and in autistic children the mirror neuron activity that is normally observed in the FOp is absent (Dapretto et al., 2006). Therefore, the molecular profile of $NOS1^+$ columns, as well as their shared location and connectivity with mirror neurons, is consistent with a potential role in motor and cognitive development.

The synthesis of NO, a short-lived gas that cannot be stored or transported, must be precisely regulated and amenable to rapid, localized activation. Because FMRP controls both the dendritic localization and translation of target mRNAs, it is well suited to contribute to the dynamic regulation of NOS1 activity. It should be noted, however, that *NOS1* mRNA may also be under additional, perhaps negative, posttranscription control, as suggested by the lack of NOS1 protein expression in the majority of *NOS1* mRNA-expressing pyramidal neurons. The modulation of neuronal function by NO in the brain has been widely studied, and postsynaptic NO is thought to represent a retrograde signal that promotes presynaptic differentiation (Bredt and Snyder, 1994; Garthwaite, 2008). Blockade of NOS1 function has been shown to disrupt synapse formation and result in spine loss (Nikonenko et al., 2008). Given the potential role of NO in synapse development, the loss of NOS1 expression in the fetal FXS brain during early synaptogenesis may contribute to the dendritic spine phenotype of human FXS (Irwin et al., 2000). Studies have also shown that NO mediates neuronal synchronization (O'Donnell and Grace, 1997) and can modulate protein function via *S*-nitrosylation (Jaffrey et al., 2001), including that of histones (Nott et al., 2008), which can mediate transcriptome changes. In future studies it will be important to characterize the mechanisms of NO function in the developing human neocortex and their potential contribution to FXS.

EXPERIMENTAL PROCEDURES

Human Brain Tissue Processing

The sources and methods for the collection, dissection, and fixation of control and fragile X postmortem human tissues are described in the Extended Experimental Procedures. All specimens were collected under guidelines approved by institutional review boards and anonymized prior to our receipt. Fixed tissues were sectioned by vibratome or cryostat. For NADPH-d staining, sections were incubated in β-NADPH, nitro blue tetrazolium, and Triton X-100. Sections were preincubated in hydrogen peroxide for immunohistochemistry or directly preblocked in blocking solution for immunofluorescent staining prior to incubation with primary antibodies followed by biotinylated or fluorophore-conjugated secondary antibodies. For immunohistochemistry, sections were further incubated in avidin-biotin-peroxidase complex and visualized using DAB.

RNA Pull-Down Assay and RIP

For pull-down assays, RNAs were transcribed from cDNA or PCR products, biotinylated, and captured using streptavidin beads. Human midfetal CP lysates were added, and bound proteins were analyzed by SDS-PAGE, silver staining, and immunoblotting. For RIP, FMRP-bound mRNAs were immunoprecipitated from midfetal human and neonatal mouse CP lysates and analyzed using quantitative RT-PCR.

Expression Assays and IUE

The generation of DNA constructs is described in the Extended Experimental Procedures. Neuro-2a cells were transfected by lipofection. Luciferase or NOS activity was assayed 48 hr after transfection and normalized to transfection efficiency controls. For electroporation, DNA was injected into the lateral ventricles of embryonic mice and transferred into VZ cells by 40V pulses. Electroporated brains were analyzed at P0 by immunostaining. All experiments using animals were carried out in accordance with a protocol approved by Yale University's Committee on Animal Research and National Institutes of Health guidelines.

SUPPLEMENTAL INFORMATION

Supplemental Information includes Supplemental Experimental Procedures and six figures and can be found with this article online at doi:10.1016/j.cell.2012.02.060.

ACKNOWLEDGMENTS

We thank D. Budinščak, Z. Cmuk, Z. Krsnik, S. Liu-Chen, B. Popović, B. Poulos, and B. Sajin for help with tissue acquisition; M. Nakane, W. Sessa, and I. Grkovic for antibodies and reagents; F. Cheng and M. Li for analyzing transcriptome data; E. Gulcicek for help with mass spectrometry; and M. Brown, L. Kaczmarek, A. Louvi, M. Günel, M. State, and members of the N.Š. laboratory for discussions and comments. E.J.H. and D.H.R. received technical support from the Pediatric Neuropathology Research Lab at

University of California, San Francisco (UCOP Award #142675). D.H.R. is a HHMI Investigator. A.M.M.S. is supported by a fellowship from the Portuguese Foundation for Science and Technology. This work was supported by grants from National Institutes of Health (to M-R.R., K99NS064303; to P.R., DA023999; to N.Ś., MH081896, MH089929, and NS054273), ZonMw 912-07-022 (to R.W.), Kavli Foundation, NARSAD, and James S. McDonnell Foundation Scholar Award (to N.Ś.).

Received: September 9, 2011
Revised: December 19, 2011
Accepted: February 15, 2012
Published: May 10, 2012

REFERENCES

Abbeduto, L., Brady, N., and Kover, S.T. (2007). Language development and fragile X syndrome: profiles, syndrome-specificity, and within-syndrome differences. Ment. Retard. Dev. Disabil. Res. Rev. *13*, 36–46.

Ashley, C.T., Jr., Wilkinson, K.D., Reines, D., and Warren, S.T. (1993). FMR1 protein: conserved RNP family domains and selective RNA binding. Science *262*, 563–566.

Bagni, C., and Greenough, W.T. (2005). From mRNP trafficking to spine dysmorphogenesis: the roots of fragile X syndrome. Nat. Rev. Neurosci. *6*, 376–387.

Bassell, G.J., and Warren, S.T. (2008). Fragile X syndrome: loss of local mRNA regulation alters synaptic development and function. Neuron *60*, 201–214.

Bechara, E.G., Didiot, M.C., Melko, M., Davidovic, L., Bensaid, M., Martin, P., Castets, M., Pognonec, P., Khandjian, E.W., Moine, H., and Bardoni, B. (2009). A novel function for fragile X mental retardation protein in translational activation. PLoS Biol. *7*, e16.

Bredt, D.S., and Snyder, S.H. (1994). Nitric oxide: a physiologic messenger molecule. Annu. Rev. Biochem. *63*, 175–195.

Brenman, J.E., Chao, D.S., Gee, S.H., McGee, A.W., Craven, S.E., Santillano, D.R., Wu, Z., Huang, F., Xia, H., Peters, M.F., et al. (1996). Interaction of nitric oxide synthase with the postsynaptic density protein PSD-95 and alpha1-syntrophin mediated by PDZ domains. Cell *84*, 757–767.

Britanova, O., de Juan Romero, C., Cheung, A., Kwan, K.Y., Schwark, M., Gyorgy, A., Vogel, T., Akopov, S., Mitkovski, M., Agoston, D., et al. (2008). Satb2 is a postmitotic determinant for upper-layer neuron specification in the neocortex. Neuron *57*, 378–392.

Brown, V., Jin, P., Ceman, S., Darnell, J.C., O'Donnell, W.T., Tenenbaum, S.A., Jin, X., Feng, Y., Wilkinson, K.D., Keene, J.D., et al. (2001). Microarray identification of FMRP-associated brain mRNAs and altered mRNA translational profiles in fragile X syndrome. Cell *107*, 477–487.

Bush, G., Frazier, J.A., Rauch, S.L., Seidman, L.J., Whalen, P.J., Jenike, M.A., Rosen, B.R., and Biederman, J. (1999). Anterior cingulate cortex dysfunction in attention-deficit/hyperactivity disorder revealed by fMRI and the Counting Stroop. Biol. Psychiatry *45*, 1542–1552.

Buxhoeveden, D., Lefkowitz, W., Loats, P., and Armstrong, E. (1996). The linear organization of cell columns in human and nonhuman anthropoid Tpt cortex. Anat. Embryol. (Berl.) *194*, 23–36.

Casanova, M.F., Buxhoeveden, D.P., Switala, A.E., and Roy, E. (2002). Minicolumnar pathology in autism. Neurology *58*, 428–432.

Chen, J.G., Rasin, M.R., Kwan, K.Y., and Sestan, N. (2005). *Zfp312* is required for subcortical axonal projections and dendritic morphology of deep-layer pyramidal neurons of the cerebral cortex. Proc. Natl. Acad. Sci. USA *102*, 17792–17797.

Chen, L., Yun, S.W., Seto, J., Liu, W., and Toth, M. (2003). The fragile X mental retardation protein binds and regulates a novel class of mRNAs containing U rich target sequences. Neuroscience *120*, 1005–1017.

Cui, H., Nishiguchi, N., Yanagi, M., Fukutake, M., Mouri, K., Kitamura, N., Hashimoto, T., Shirakawa, O., and Hishimoto, A. (2010). A putative cis-acting polymorphism in the *NOS1* gene is associated with schizophrenia and NOS1 immunoreactivity in the postmortem brain. Schizophr. Res. *121*, 172–178.

Dapretto, M., Davies, M.S., Pfeifer, J.H., Scott, A.A., Sigman, M., Bookheimer, S.Y., and Iacoboni, M. (2006). Understanding emotions in others: mirror neuron dysfunction in children with autism spectrum disorders. Nat. Neurosci. *9*, 28–30.

Darnell, J.C., Jensen, K.B., Jin, P., Brown, V., Warren, S.T., and Darnell, R.B. (2001). Fragile X mental retardation protein targets G quartet mRNAs important for neuronal function. Cell *107*, 489–499.

Darnell, J.C., Van Driesche, S.J., Zhang, C., Hung, K.Y., Mele, A., Fraser, C.E., Stone, E.F., Chen, C., Fak, J.J., Chi, S.W., et al. (2011). FMRP stalls ribosomal translocation on mRNAs linked to synaptic function and autism. Cell *146*, 247–261.

Dawson, T.M., Bredt, D.S., Fotuhi, M., Hwang, P.M., and Snyder, S.H. (1991). Nitric oxide synthase and neuronal NADPH diaphorase are identical in brain and peripheral tissues. Proc. Natl. Acad. Sci. USA *88*, 7797–7801.

Devinsky, O., Morrell, M.J., and Vogt, B.A. (1995). Contributions of anterior cingulate cortex to behaviour. Brain *118*, 279–306.

Dictenberg, J.B., Swanger, S.A., Antar, L.N., Singer, R.H., and Bassell, G.J. (2008). A direct role for FMRP in activity-dependent dendritic mRNA transport links filopodial-spine morphogenesis to fragile X syndrome. Dev. Cell *14*, 926–939.

The Dutch-Belgian Fragile X Consortium. (1994). *Fmr1* knockout mice: a model to study fragile X mental retardation. Cell *78*, 23–33.

Fertuzinhos, S., Krsnik, Z., Kawasawa, Y.I., Rasin, M.R., Kwan, K.Y., Chen, J.G., Judas, M., Hayashi, M., and Sestan, N. (2009). Selective depletion of molecularly defined cortical interneurons in human holoprosencephaly with severe striatal hypoplasia. Cereb. Cortex *19*, 2196–2207.

Garthwaite, J. (2008). Concepts of neural nitric oxide-mediated transmission. Eur. J. Neurosci. *27*, 2783–2802.

Geschwind, D.H., and Levitt, P. (2007). Autism spectrum disorders: developmental disconnection syndromes. Curr. Opin. Neurobiol. *17*, 103–111.

Ho, G.P., Selvakumar, B., Mukai, J., Hester, L.D., Wang, Y., Gogos, J.A., and Snyder, S.H. (2011). S-nitrosylation and S-palmitoylation reciprocally regulate synaptic targeting of PSD-95. Neuron *71*, 131–141.

Hope, B.T., Michael, G.J., Knigge, K.M., and Vincent, S.R. (1991). Neuronal NADPH diaphorase is a nitric oxide synthase. Proc. Natl. Acad. Sci. USA *88*, 2811–2814.

Iioka, H., Loiselle, D., Haystead, T.A., and Macara, I.G. (2011). Efficient detection of RNA-protein interactions using tethered RNAs. Nucleic Acids Res. *39*, e53.

Irwin, S.A., Galvez, R., and Greenough, W.T. (2000). Dendritic spine structural anomalies in fragile-X mental retardation syndrome. Cereb. Cortex *10*, 1038–1044.

Jaffrey, S.R., Erdjument-Bromage, H., Ferris, C.D., Tempst, P., and Snyder, S.H. (2001). Protein S-nitrosylation: a physiological signal for neuronal nitric oxide. Nat. Cell Biol. *3*, 193–197.

Johnson, M.B., Kawasawa, Y.I., Mason, C.E., Krsnik, Z., Coppola, G., Bogdanović, D., Geschwind, D.H., Mane, S.M., State, M.W., and Sestan, N. (2009). Functional and evolutionary insights into human brain development through global transcriptome analysis. Neuron *62*, 494–509.

Judas, M., Sestan, N., and Kostović, I. (1999). Nitrinergic neurons in the developing and adult human telencephalon: transient and permanent patterns of expression in comparison to other mammals. Microsc. Res. Tech. *45*, 401–419.

Kang, H.J., Kawasawa, Y.I., Cheng, F., Zhu, Y., Xu, X., Li, M., Sousa, A.M.M., Pletikos, M., Meyer, K.A., Sedmak, G., et al. (2011). Spatio-temporal transcriptome of the human brain. Nature *478*, 483–489.

Keller, S.S., Crow, T., Foundas, A., Amunts, K., and Roberts, N. (2009). Broca's area: nomenclature, anatomy, typology and asymmetry. Brain Lang. *109*, 29–48.

Kostovic, I., and Rakic, P. (1990). Developmental history of the transient subplate zone in the visual and somatosensory cortex of the macaque monkey and human brain. J. Comp. Neurol. *297*, 441–470.

Kraskov, A., Dancause, N., Quallo, M.M., Shepherd, S., and Lemon, R.N. (2009). Corticospinal neurons in macaque ventral premotor cortex with mirror properties: a potential mechanism for action suppression? Neuron *64*, 922–930.

Kwan, K.Y., Lam, M.M., Krsnik, Z., Kawasawa, Y.I., Lefebvre, V., and Sestan, N. (2008). SOX5 postmitotically regulates migration, postmigratory differentiation, and projections of subplate and deep-layer neocortical neurons. Proc. Natl. Acad. Sci. USA *105*, 16021–16026.

Lai, C.S., Fisher, S.E., Hurst, J.A., Vargha-Khadem, F., and Monaco, A.P. (2001). A forkhead-domain gene is mutated in a severe speech and language disorder. Nature *413*, 519–523.

Leone, D.P., Srinivasan, K., Chen, B., Alcamo, E., and McConnell, S.K. (2008). The determination of projection neuron identity in the developing cerebral cortex. Curr. Opin. Neurobiol. *18*, 28–35.

Lui, J.H., Hansen, D.V., and Kriegstein, A.R. (2011). Development and evolution of the human neocortex. Cell *146*, 18–36.

Menon, V., Leroux, J., White, C.D., and Reiss, A.L. (2004). Frontostriatal deficits in fragile X syndrome: relation to FMR1 gene expression. Proc. Natl. Acad. Sci. USA *101*, 3615–3620.

Molliver, M.E., Kostović, I., and van der Loos, H. (1973). The development of synapses in cerebral cortex of the human fetus. Brain Res. *50*, 403–407.

Molyneaux, B.J., Arlotta, P., Menezes, J.R., and Macklis, J.D. (2007). Neuronal subtype specification in the cerebral cortex. Nat. Rev. Neurosci. *8*, 427–437.

Mountcastle, V.B. (1997). The columnar organization of the neocortex. Brain *120*, 701–722.

Nikonenko, I., Boda, B., Steen, S., Knott, G., Welker, E., and Muller, D. (2008). PSD-95 promotes synaptogenesis and multiinnervated spine formation through nitric oxide signaling. J. Cell Biol. *183*, 1115–1127.

Nott, A., Watson, P.M., Robinson, J.D., Crepaldi, L., and Riccio, A. (2008). S-Nitrosylation of histone deacetylase 2 induces chromatin remodelling in neurons. Nature *455*, 411–415.

O'Donnell, P., and Grace, A.A. (1997). Cortical afferents modulate striatal gap junction permeability via nitric oxide. Neuroscience *76*, 1–5.

Peters, A. (2010). The morphology of minicolumns. In The Neurochemical Basis of Autism: from Molecules to Minicolumns, G.J. Blatt, ed. (New York: Springer), pp. 45–68.

Pierce, K., and Redcay, E. (2008). Fusiform function in children with an autism spectrum disorder is a matter of "who". Biol. Psychiatry *64*, 552–560.

Power, J.D., Cohen, A.L., Nelson, S.M., Wig, G.S., Barnes, K.A., Church, J.A., Vogel, A.C., Laumann, T.O., Miezin, F.M., Schlaggar, B.L., et al. (2011). Functional network organization of the human brain. Neuron *72*, 665–678.

Rackham, O., and Brown, C.M. (2004). Visualization of RNA-protein interactions in living cells: FMRP and IMP1 interact on mRNAs. EMBO J. *23*, 3346–3355.

Rakic, P. (1988). Specification of cerebral cortical areas. Science *241*, 170–176.

Ramocki, M.B., and Zoghbi, H.Y. (2008). Failure of neuronal homeostasis results in common neuropsychiatric phenotypes. Nature *455*, 912–918.

Reif, A., Herterich, S., Strobel, A., Ehlis, A.C., Saur, D., Jacob, C.P., Wienker, T., Töpner, T., Fritzen, S., Walter, U., et al. (2006). A neuronal nitric oxide synthase (NOS-I) haplotype associated with schizophrenia modifies prefrontal cortex function. Mol. Psychiatry *11*, 286–300.

Reif, A., Jacob, C.P., Rujescu, D., Herterich, S., Lang, S., Gutknecht, L., Baehne, C.G., Strobel, A., Freitag, C.M., Giegling, I., et al. (2009). Influence of functional variant of neuronal nitric oxide synthase on impulsive behaviors in humans. Arch. Gen. Psychiatry *66*, 41–50.

Rizzolatti, G., and Craighero, L. (2004). The mirror-neuron system. Annu. Rev. Neurosci. *27*, 169–192.

Rogers, S.J., Wehner, D.E., and Hagerman, R. (2001). The behavioral phenotype in fragile X: symptoms of autism in very young children with fragile X syndrome, idiopathic autism, and other developmental disorders. J. Dev. Behav. Pediatr. *22*, 409–417.

Schaeffer, C., Bardoni, B., Mandel, J.L., Ehresmann, B., Ehresmann, C., and Moine, H. (2001). The fragile X mental retardation protein binds specifically to its mRNA via a purine quartet motif. EMBO J. *20*, 4803–4813.

Sestan, N., and Kostović, I. (1994). Histochemical localization of nitric oxide synthase in the CNS. Trends Neurosci. *17*, 105–106.

Shinkai, T., Ohmori, O., Hori, H., and Nakamura, J. (2002). Allelic association of the neuronal nitric oxide synthase (*NOS1*) gene with schizophrenia. Mol. Psychiatry *7*, 560–563.

Siomi, H., Choi, M., Siomi, M.C., Nussbaum, R.L., and Dreyfuss, G. (1994). Essential role for KH domains in RNA binding: impaired RNA binding by a mutation in the KH domain of FMR1 that causes fragile X syndrome. Cell *77*, 33–39.

State, M.W. (2010). The genetics of child psychiatric disorders: focus on autism and Tourette syndrome. Neuron *68*, 254–269.

Todd, P.K., Mack, K.J., and Malter, J.S. (2003). The fragile X mental retardation protein is required for type-I metabotropic glutamate receptor-dependent translation of PSD-95. Proc. Natl. Acad. Sci. USA *100*, 14374–14378.

Tu, P.C., Hsieh, J.C., Li, C.T., Bai, Y.M., and Su, T.P. (2012). Cortico-striatal disconnection within the cingulo-opercular network in schizophrenia revealed by intrinsic functional connectivity analysis: a resting fMRI study. Neuroimage *59*, 238–247.

Walsh, C.A., Morrow, E.M., and Rubenstein, J.L. (2008). Autism and brain development. Cell *135*, 396–400.

Willemsen, R., Levenga, J., and Oostra, B.A. (2011). CGG repeat in the FMR1 gene: size matters. Clin. Genet. *80*, 214–225.

Zalfa, F., Eleuteri, B., Dickson, K.S., Mercaldo, V., De Rubeis, S., di Penta, A., Tabolacci, E., Chiurazzi, P., Neri, G., Grant, S.G., and Bagni, C. (2007). A new function for the fragile X mental retardation protein in regulation of PSD-95 mRNA stability. Nat. Neurosci. *10*, 578–587.

Cell

EXTENDED EXPERIMENTAL PROCEDURES

Control and Fragile X Syndrome Human Brain Tissues

This study was conducted using postmortem human brain specimens from tissue collections at the Department of Neurobiology at Yale School of Medicine. Additional specimens were procured from the Human Fetal Tissue Repository at the Albert Einstein College of Medicine, New York City; Erasmus MC, University Medical Center, Rotterdam; Department of Pathology at the University of California, San Francisco; and the NICHD Brain and Tissue Bank for Developmental Disorders at the University of Maryland, Baltimore. Tissue was collected under guidelines approved by the institutional review boards at the Yale University School of Medicine and the respective institutions from which tissue specimens were obtained. Appropriate informed consent was obtained from parents or next-of-kin, all specimens were anonymized prior to our receipt, and available nonidentifying data were recorded. The PCW age of human specimens was determined based on the date of the mother's last menstruation, ultrasound data, crown-rump length, foot length, or brain weight. For control specimens, only brains from clinically unremarkable donors and with no signs of prolonged agonal conditions, obvious malformations, significant hemorrhages, brain lesions, or perinatal lesions were used. For postnatal FXS specimens, only brains without prolonged agonal conditions or significant hemorrhages were used. All tissues were processed in accordance with ethical guidelines and regulations for the research use of human brain tissue set forth by the NIH and the WMA Declaration of Helsinki.

For quantitative RT-PCR analysis and immunoblotting, the neocortex of fresh frozen control (15 and 19 PCW; and 8, 22, and 82 postnatal years) and FXS specimens (15 and 18 PCW; 9, 22, and 85 postnatal years) were dissected on an aluminum plate over dry ice under a dissecting microscope. Meninges, subplate, and white matter were careful removed. A lysate from each sample was divided for quantitative RT-PCR analysis and immunoblotting as described below. The exact postconceptional age of one of the FXS specimens was not known, but was estimated based on anatomical features to be around 15 PCW. For RNA pull-down and RIP assays, frozen tissue blocks from a 21 PCW control cortex were dissected as described above and thawed on ice immediately prior to use.

For fixed control specimens, tissue blocks were immersed in cold 4% paraformaldehyde (PFA) in 0.1 M phosphate buffer, pH 7.4 (PB) for 24-72 hr with gentle shaking. After fixation, blocks were washed in 0.1 M phosphate-buffered saline (PBS) and stored in PBS with 0.02% sodium azide at 4°C or cryoprotected in graded sucrose solutions, flash-frozen in dry-ice cooled isopentane, and stored at −80°C. Sections 50–120 μm in thickness were obtained using a vibratome (Leica VT1000S) or cryostat (Leica CM3050S).

In addition, we analyzed existing tissue sections of control pre- and postnatal stained human brain specimens stained for NADPH-d histochemistry and NOS1 immunohistochemistry that are part of the Zagreb Neuroembryological Collection at the Croatian Institute for Brain Research and University of Zagreb School of Medicine, Zagreb (Judaš et al., 2011).

The postmortem intervals for all fixed control specimens were between 0.5 to 25 hr and ranged in age from 12 to 37 PCW for fetal specimens (N = 34); postnatal day (P) 2 to 12 years for early postnatal specimens (N = 14); and 20 to 64 years for adults (N = 8).

Macaque Monkey and Mouse Brain Tissues

All experiments using animals were carried out in accordance with a protocol approved by Yale University's Committee on Animal Research and NIH guidelines. *Macaca mulatta* ranged in age from embryonic day (E) 60 to E140 (N = 17) for fetal specimens; P 14 to 7 years for early postnatal specimens (N = 8); and 8 to 22 years for adults (N = 7). Postnatal brains were perfused with heparinized saline followed by either 4% PFA, 0.08% glutaraldehyde, and 0.2% picric acid in PB or 4% PFA in PB, dissected into coronally oriented blocks, and postfixed by immersion in fixative for 6 hr. All prenatal and two postnatal brains were dissected without perfusion, flushed with heparinized saline, and fixed by 4% PFA immersion for 24-36 hr.

For mouse tissue, dissected brains of embryonic day (E) 14.5, 16.5, 18.5 and postnatal day (P) 0, 3, 4, 7, 14, and adult (>3 month-old) were fixed by immersion in 4% PFA for 16-24 hr. After fixation, tissues were washed with PBS and stored in PBS with sodium azide at 4°C or cryoprotected, flash-frozen, and stored at −80°C. Sections 60–100 μm in thickness were obtained using a vibratome or cryostat. For RIP assays, dissected cortices were rapidly frozen on dry ice without fixation and thawed on ice immediately prior to use. *Fmr1* mutant mice (The Dutch-Belgian Fragile X Consortium, 1994) were obtained from the Jackson laboratory and genotyped with the following primers:

Fmr1_mut_F, cacgagactagtgagacgtg
Fmr1_WT_F, tgtgatagaatatgcagcatgtga
Fmr1_common_R, cttctggcacctccagctt

NADPH-Diaphorase Histochemistry

Free-floating vibratome or frozen sections 50-120 μm in thickness were incubated in 1 mM beta-NADPH (Sigma), 0.8 mM nitro blue tetrazolium (Sigma), and 0.3% Triton X-100 in 0.1 M PBS (pH 8.0) at 37°C for 3-10 hr in the dark. After incubation, sections were washed three times in PBS, briefly rinsed in warm (55°C) dimethylformamide to reduce background staining. Sections were mounted on Superfrost Plus charged slides, dehydrated, and coverslipped with Permount (Fisher Scientific) and imaged with a light microscope (Zeiss) or scanned with a digital scanner (Scanscope, Aperio).

Antibodies

For immunostaining, the following primary antibodies were used at the indicated dilution: anti-NOS1 (rabbit, 1:200; Zymed/Invitrogen, 61-7000), anti-NOS1 (mouse, 1:100; Santa Cruz Biotechnology, sc-5302), anti-BCL11B/CTIP2 (rat, 1:250; Santa Cruz Biotechnology, sc-56014), anti-SATB2 (mouse, 1:200; GenWay Biotech, 20-372-60065), anti-FOXP2 (rabbit, 1:20000; Abcam, ab16046), anti-cFOS (mouse, 1:250; Santa Cruz Biotechnology, sc-8047), anti-SYP (mouse, 1:250; Sigma-Aldrich, S5768), anti-CUX1 (rabbit, 1:150; Santa Cruz Biotechnology, sc-13024), anti-POU3F2/BRN2 (goat, 1:250; Santa Cruz Biotechnology, sc-6029), anti-FMRP (mouse, 1:200; Chemicon/Millipore, MAB2160), anti-FMRP (rabbit, 1:250; Santa Cruz Biotechnology, sc-28739), and anti-VIM (goat. 1:250; Santa Cruz Biotechnology, sc-7557). For immunoblotting: anti-NOS1 (mouse, 1:5000; Santa Cruz Biotechnology, sc-5302), anti-FMRP (rabbit, 1:1000; Santa Cruz Biotechnology, sc-28739 and rabbit, 1:1000; Abcam, ab17722), anti-GAPDH (rabbit, 1:5000; Abcam, ab9485), anti-CPEB3 (rabbit, 1:500; Abcam, ab10883), anti-EIF2C2/AGO2 (rabbit, 1:500; Abcam, ab32381), anti-PABP (rabbit, 1:200; Santa Cruz Biotechnology, sc-28834), and anti-FXR1 (rabbit, 1:1000; Cell Signaling Technology, 4264).

Immunohistochemistry and Immunofluorescent Staining

Free-floating vibratome or cryo-sections 60-100 μm in thickness were either first preincubated in 1% hydrogen peroxide (for immunohistochemistry) or directly incubated (for immunofluorescent staining) in blocking solution (BS) containing 5% normal donkey serum (Jackson ImmunoResearch Laboratories), 1% bovine serum albumin, 0.1% glycine, 0.1% lysine, 0.4% Triton X-100 for one hour at room temperature. After preblocking, sections were incubated in primary antibodies diluted in BS for 24-72 hr at 4°C. After washing in PBS, sections were incubated with biotinylated (for immunohistochemistry) or fluorophore-conjugated (for immunofluorescent staining) secondary antibodies raised in donkey (Jackson ImmunoResearch) diluted in BS for 2-4 hr at room temperature or 16 hr at 4°C. For immunofluorescent staining, sections were counterstained with DAPI and mounted in Vectashield (Vector laboratories) and imaged using a confocal microscope (LSM 510, Zeiss). For immunohistochemistry, sections were further incubated in avidin-biotin-peroxidase complex (Vectastain ABC Elite kit, Vector laboratories) for 2 hr at room temperature. Peroxidase activity was visualized using a DAB peroxidase substrate kit (Vector Laboratories). Sections were mounted on Superfrost Plus charged slides, dehydrated, coverslipped with Permount and imaged with a light microscope or scanned.

Electron Microscopic Immunohistochemistry

For immunoelectron microscopy, vibratome sections 70 μm in thickness were cryoprotected in 30% sucrose and freeze-thawed in liquid nitrogen three times, washed, and processed for DAB immunohistochemistry as described above without Triton X-100 permeabilization. After washes in PBS, sections were osmificated with 1% osmium tetroxide, dehydrated in an ethanol series, and flat-embedded in Durcupan (Fluka) on liquid release pretreated slides. Areas of interest were dissected with a surgical blade, examined under a light microscope, and sectioned using an ultramicrotome (Reichert). The resulting ultrathin sections were collected on slot grids, stained with lead citrate and uranyl acetate, and imaged with a JEOL 1010 transmission microscope (JEOL).

Quantitative Analysis

Data were analyzed by two-tailed Student's t test with a significance level of at least $p < 0.05$ for all statistical comparisons. The numbers of biological and experimental replicates are indicated in the text or figure legends. Analysis of the spatial distribution of NADPH-d positive neurons was performed under a light microscope (Zeiss) using Stereo Investigator (Microbrightfield). Analyses of columnarity were performed as previously described (Buxhoeveden et al., 1996).

Retrograde Axonal Tracing

To retrogradely trace axonal projections, a fixed human 20 PCW brain was cut into coronal slabs. In the block containing the FOp and ACC, small crystals (30-70 μm in diameter) of fluorescent dye FAST DiI (Molecular Probes) were inserted into the internal capsule at the level of the septum, and FAST DiA into the anterior part of the corpus callosum. After incubation in 4% PFA in the dark at 37°C for seven months, the block was cut, embedded in gelling temperature agarose, and sectioned on a vibratome at 100 μm. Images were acquired using a confocal microscope (LSM 510; Zeiss).

RNA In Situ Hybridization

Free-floating or slide-mounted cryosections 60 μm in thickness were postfixed in 4% PFA for 15 min, washed, and hybridized overnight at 70°C with 500 ng/ml of digoxigenin (DIG)-labeled cRNA probes corresponding to nucleotides 2888–3648 of mouse *Nos1* (NM_008712), 793-1085 of human *NOS1* (NM_000620) and 361–1506 of human *FEZF2* (NM_018008). The signal was detected with an alkaline phosphatase-conjugated anti-DIG antibody and NBT/BCIP chromogen (Roche).

Fluorescence-Activated Cell Sorting

To isolate cells derived from the *Emx1* lineage, which encompasses all cortical pyramidal neurons but does not include any interneurons, the neocortices of P3 mice doubly transgenic for *Emx1-Cre* and *CAG-Cat-Gfp* were dissected, minced, and enzymatically dissociated. Dissociated cells were sorted by GFP fluorescence using the FACSAria II cell sorter (BD Biosciences). Total RNA was extracted from separately collected GFP^+ and GFP^- cells using Trizol (Invitrogen) and further purified using the RNeasy MinElute

clean up kit (QIAGEN). RNAs were quantified (Nanodrop), reverse transcribed using Superscript II (Invitrogen), and analyzed for *Nos1* and *Gapdh* levels using Taqman expression assays (Applied Biosystems) with the ABI Prism 7900 qPCR system.

RNA Pull-Down Assay

Full length RNAs for *NOS1*, *GAPDH*, *EGFP*, and *NeoR*, were transcribed in vitro from cDNA plasmids using the HiScribe kit (New England Biolabs). DNA fragments representing the predicted FMRP binding sites in *NOS1* (GQ1-3 and UR1-6) were PCR amplified using the following primers:

NOS1_GQ1_F, gtattataatacgactcactatagggagaaagaccatccgggtgaca
NOS1_GQ1_R, gagtgagccagcctcctg
NOS1_GQ2_F, gtattataatacgactcactatagggagaaaggcagaggggagaacaat
NOS1_GQ2_R, gggcagaggtttgtgtgact
NOS1_GQ3_F, gtattataatacgactcactatagggagagaagaccctcaatgccaaga
NOS1_GQ3_R, gggagacagccccttaatc
NOS1_UR1_F, gtattataatacgactcactatagggagaaactcacgggtgcatgaaa
NOS1_UR1_R, ggactggctcagagagcttg
NOS1_UR2_F, gtattataatacgactcactatagggagagtccctcagccactgaagtc
NOS1_UR2_R, agaggacggacagagacctg
NOS1_UR3_F, gtattataatacgactcactatagggagattaaagctttggtgcctgga
NOS1_UR3_R, tccactttaaccagcttccatt
NOS1_UR4_F, gtattataatacgactcactatagggagatcctccctaagaggcaacct
NOS1_UR4_R, ctttctgggaactgcctgac
NOS1_UR5_F, gtattataatacgactcactatagggagatctcattttgtcaaggagtcca
NOS1_UR5_R, tagcctggagttgtgaagca
NOS1_UR6_F, gtattataatacgactcactatagggagaaacacagttcctctcgtgcag
NOS1_UR6_R, gaactgggggaggcagag

The RNA pull-down assay was carried out using a protocol similar to one previously described (Lee et al., 2010). Briefly, RNAs were transcribed from PCR products. After treatment with DNase (Ambion) and column purification (QIAGEN), the RNAs were biotinylated with biotin-ATP (Perkin Elmer) using poly(A) polymerase (New England Biolabs), and re-purified. Biotinylated RNAs were captured using streptavidin dynabeads (M-280, Invitrogen) according to manufacturer's instructions. Unbound RNAs were removed by extensive washing. For cortical lysates, dissected neocortical plate of 20 and 21 PCW fetal brains was placed in polysome extraction buffer (20 mM Tris-HCl, 100 mM KCl, 5 mM MgCl2, 0.5% NP-40, pH 7.5) supplemented with RNase and protease inhibitors (Roche) and dissociated using precleaned steel beads and a bullet blender (Next Advance). After centrifugation, the supernatant was precleared with M-280 Dynabeads, supplemented with 0.1 mg/ml yeast tRNA (Invitrogen), and incubated with the immobilized RNA. After extensive washing with polysome extraction buffer, bound proteins were eluted with 1X SDS loading buffer, resolved by SDS-PAGE, and analyzed by silver staining and immunoblotting.

RNA-Binding Protein Immunoprecipitation

For RNA-binding protein immunoprecipitation (RIP), a rabbit polyclonal anti-FMRP antibody (H-120, Santa Cruz Biotechnology, sc-28739) was used since the commonly used mouse monoclonal antibody (7G1-1) does not recognize human FMRP. All procedures were performed according to a previously described protocol from the Kindler laboratory (Iacoangeli et al., 2008). Briefly, approximately 0.5g of fresh frozen neocortex was homogenized in cold lysis buffer (10 mM HEPES, 200 mM NaCl, 30 mM EDTA, 0.5% Triton X-100) supplemented with RNase and protease inhibitors (Roche) by stainless steel beads using a bullet blender (Next Advance). The supernatant was collected after centrifugation and incubated for 6 hr at 4°C with 15 μg of rabbit polyclonal anti-FMRP antibody or control rabbit IgG (Santa Cruz Biotechnology). Antibodies and bound complexes were then captured by incubation with 100 μl of protein A/G Dynabeads (Invitrogen), which were preblocked with 0.1 μg/ml of BSA, glycogen, and yeast tRNA, at 4°C for 2 to 4 hr. After extensive washes with PBS, captured RNAs were eluted using Trizol (Invitrogen) and further purified using the RNeasy MinElute clean up kit (QIAGEN). RNAs were quantified (Nanodrop), reverse transcribed using Superscript II (Invitrogen), and analyzed using Taqman expression assays (Applied Biosystems) with the ABI Prism qPCR system.

RNA Electrophoretic Mobility Shift Assay

A fragment of RNA containing both GQ1 and GQ2 was prepared by T7 transcription with a biotin RNA labeling mix (Roche) from a PCR product amplified using the following primers:

hNOS1_GQs_Emsa_F, gtattataatacgactcactatagggagaaccaaagccgtggatctgt
hNOS1_GQs_Emsa_R, ttgccgtccaaatctctgtc

The RNA was purified using a G-50 sephadex column (Roche). FMRP protein was prepared from a full-length human *FMR1* cDNA (BC086957) using the TNT Quick coupled transcription/translation kit (Promega). Biotinylated and nonbiotinylated ("cold") probes were incubated with FMRP protein in an RNA-binding buffer (10 mM HEPES, 20 mM KCl, 1 mM DTT, 1 mM MgCl, 6% glycerol, 1 μg yeast tRNA) at room temperature for 30 min. The shift assay was analyzed using a 6% polyacrylamide gel (Invitrogen). The resolved labeled RNA was transferred on a nitrocellulose membrane (Biorad) and detected using the Chemiluminescent Nucleic Acid Detection Module (Thermo Scientific) according to manufacturers' instructions.

Reverse-Transcription Termination Assay

DNAs representing GQ1 and GQ2, respectively, were amplified by PCR using the following primers:

NOS1_GQ1_RT_F, gtattataatacgactcactatagggagaccaaagccgtggatctgt
NOS1_GQ1_RT_R, ttggcatgggggagtg
NOS1_GQ2_RT_F, gtattataatacgactcactatagggagaggcagaggggagaacaatg
NOS1_GQ2_RT_R, tgtgacttgccgtccaaa

RNAs were transcribed in vitro from PCR products using the HiScribe Kit (New England Biolabs). Reverse transcription was carried out using the 3′ PCR primer and AMV reverse transcriptase using a protocol similar to one previously described (Schaeffer et al., 2001). After reverse transcription, RNAs were digested using RNaseA and RNaseH and the remaining DNA fragments were resolved on a denaturing 15% polyacrylamide TBE-Urea gel (Invitrogen). DNA bands were stained using SYBR gold (Invitrogen).

Colorimetric NOS Assay

CAG-h*NOS1*, CAG-h*FMR1*, and CAG-m*Nos1* were generated by inserting the coding sequences of human *NOS1* cDNA (L02881) and *FMR1* cDNA (BC086957), and mouse *Nos1* cDNA (BC167235) into CAGEN. CAG-murinized h*NOS1* was generated by inserting, in frame, a custom synthesized DNA fragment (Integrated DNA Technologies) representing the mouse sequence orthologous to the human GQ region into the *BclI* sites of CAG-h*NOS1*. CAG-h*FMR1*(I304N) was generated by subcloning the *EcoRI* to *SphI* fragment of FMRP I304N-EGFP (Schrier et al., 2004) into CAG-h*FMR1*. Neuro-2a cells were plated in 24-well plates and transfected with Lipofectamine 2000 (Invitrogen) as previously described (Abelson et al., 2005). For each well, a total of 0.85 μg of maxi-prep (QIAGEN) plasmid DNA were transfected. 0.05 μg of firefly luciferase plasmid (SV40-GL3) was used as a transfection efficiency control. 0, 0.15, 0.35, or 0.5 μg of CAG-h*FMR1* was transfected along with 0.3 μg of CAG-h*NOS1* and varying amounts of CAG-empty to equalize the total amount of DNA transfected per well. Forty-eight hours after transfection, the cells were lysed and analyzed for luciferase activity (Promega). Aliquots of lysates containing identical levels of luciferase activity were used for the colorimetric NOS assay (Oxford Biomedical Research), which was performed according to the manufacturer's instructions.

Luciferase Assay

Luciferase plasmids SV40-GL3-h*NOS1*-GQ and SV40-GL3-m*Nos1*-GQortholog were generated by inserting into the *XbaI* site of SV40-GL3 (Promega) PCR products amplified using the following primers:

hNOS1_GQs_GL3_F, gggttctagaaccaaagccgtggatctgt
hNOS1_GQs_GL3_R, ttgttctagagtgacttgccgtccaaatct
mNos1_GQortholog_GL3_F, ggtatctagaccaaagctgtcgatctgtctc
mNos1_GQortholog_GL3_R, gagctctagacagtttgccgtcgaggtct

CAG-m*Fmr1* was generated by inserting the coding sequence of mouse *Fmr1* cDNA (BC079671) into CAGEN. Neuro-2a cells were plated in 24-well plates and transfected with Lipofectamine 2000 (Invitrogen) as previously described (Han et al., 2011). For each well, a total of 0.85 μg of DNA were transfected. 0.05 μg of renilla luciferase (pRL-SV40) was used to normalize for transfection efficiency. 0, 0.15, 0.35, or 0.5 μg of CAG-h*FMR1* or CAG-m*Fmr1*, along with varying amounts of CAG-empty to equalize final DNA content, were co-transfected with 0.3 μg of SV40-GL3-empty, SV40-GL3-h*NOS1*-GQs, or SV40-GL3-m*Nos1*-GQortholog. Forty-eight hours after transfection, the cells were lysed and analyzed for luciferase activity using the dual luciferase kit (Promega).

In Utero Electroporation

Timed-pregnancies were obtained by observation of a vaginal plug. In utero electroporations were carried out at E13.5. Two μl of a carefully quantified (Nanodrop) endotoxin-free maxiprep (QIAGEN) plasmid DNA mix containing 0.5 μg/μl of CAG-*Gfp* and 4 μg/μl of one of CAG-empty, CAG-m*Nos1*, CAG-h*NOS1* or CAG-murinized h*NOS1* was injected into the lateral ventricles and transferred into ventricular zone cells by electroporation with five 50 ms pulses of 40 V at 950 ms intervals. Electroporated brains were analyzed at P 0. To facilitate the analysis of NOS1 expression levels, all immunostaining analyses were performed using the same master mix of primary and secondary antibodies and imaged with identical parameters with a confocal microscope.

Neuronal Cell Culture and Transfection

For neuronal cultures, E14.5 neocortex from *Fmr1* KO and strain-matched wild-type controls was microdissected from embryos of timed-pregnant dams. Cells were mechanically and enzymatically dissociated, counted, and nucleofected with CAG-h*NOS1* and

transfection control SV40-GL3 using the mouse neural stem cell nucleofector kit (VPG-1004, Lonza). Cells were cultured on glass coverslips coated with laminin (Invitrogen) in 24-well plates in Neurobasal media (Invitrogen) supplemented with B-27 (Invitrogen) in the presence of FGF-2 (20 ng/ml, Millipore) and epidermal growth factor (20 ng/ml, Millipore) for 24 hr. Growth factors were then withdrawn to allow for neuronal differentiation. Forty-eight hours later, the cultured neurons were lysed and assayed for luciferasea activity. Lysates containing equal amounts of luciferase activity were analyzed for NOS1 expression by immunoblotting.

GQ Scores and Sequence Alignment

The full-length *NOS1* coding sequences of 21 species were obtained from Ensembl or UCSC genome browser. DNA and protein sequences were aligned using ClustalW2 using default parameters. Indels were removed. G quadruplex scores were determined using the QGRS Mapper (Kikin et al., 2006) under default parameters.

Topographical MRI Reconstruction

Four ex vivo fetal human brains (aged 13, 20, 30 and 40 PCW) that are part of Zagreb Collection of human brains (Judaš et al., 2011) and one adult brain (28 years old), all without any sign of pathology, were scanned with clinical 3T Siemens Trio MRI scanner using the following parameters: repetition time (TR) 14.5 ms, echo time (TE) 5.4 ms, number of excitations (NEX) 5, flip angle of 12°, acquisition time app. 1.5h per brain and section thickness ranging from 0.3-0.5 mm, depending on the age. All brains were scanned using the wrist small-flexi 8-channel coil and T1 weighted commercially available volumetric interpolated brain examination sequence. The matrix size and the field of view were adjusted to obtain an isotropic spatial resolution complementary to the slice thickness of at least 0.3 × 0.3 mm^2 for 13 PCW fetal brains, and 0.5 × 0.5 mm^2 for the fetal brains older than 15 PCW. The surfaces of the cortical plate (13-40 PCW) and cerebral cortex (28 years) were reconstructed as a last step of image processing using the semi-automated pipeline for processing fetal and adult postmortem brain MR images that has been established and developed at Montreal Neurological Institute ACE lab (http://www.bic.mni.mcgill.ca/~alan/tools.html).

SUPPLEMENTAL REFERENCES

Abelson, J.F., Kwan, K.Y., O'Roak, B.J., Baek, D.Y., Stillman, A.A., Morgan, T.M., Mathews, C.A., Pauls, D.L., Rasin, M.R., Gunel, M., et al. (2005). Sequence variants in SLITRK1 are associated with Tourette's syndrome. Science *310*, 317–320.

DeFelipe, J., Alonso-Nanclares, L., and Arellano, J.I. (2002). Microstructure of the neocortex: comparative aspects. J. Neurocytol. *31*, 299–316.

Han, W., Kwan, K.Y., Shim, S., Lam, M.M., Shin, Y., Xu, X., Zhu, Y., Li, M., and Sestan, N. (2011). TBR1 directly represses Fezf2 to control the laminar origin and development of the corticospinal tract. Proc. Natl. Acad. Sci. USA *108*, 3041–3046.

Iacoangeli, A., Rozhdestvensky, T.S., Dolzhanskaya, N., Tournier, B., Schütt, J., Brosius, J., Denman, R.B., Khandjian, E.W., Kindler, S., and Tiedge, H. (2008). On BC1 RNA and the fragile X mental retardation protein. Proc. Natl. Acad. Sci. USA *105*, 734–739.

Judaš, M., Šimić, G., Petanjek, Z., Jovanov-Milošević, N., Pletikos, M., Vasung, L., Vukšić, M., and Kostović, I. (2011). The Zagreb Collection of human brains: a unique, versatile, but underexploited resource for the neuroscience community. Ann. N Y Acad. Sci. *1225* (*Suppl 1*), E105–E130.

Kikin, O., D'Antonio, L., and Bagga, P.S. (2006). QGRS Mapper: a web-based server for predicting G-quadruplexes in nucleotide sequences. Nucleic Acids Res. *34* (*Web Server issue*), W676–W82.

Lee, E.K., Kim, H.H., Kuwano, Y., Abdelmohsen, K., Srikantan, S., Subaran, S.S., Gleichmann, M., Mughal, M.R., Martindale, J.L., Yang, X., et al. (2010). hnRNP C promotes APP translation by competing with FMRP for APP mRNA recruitment to P bodies. Nat. Struct. Mol. Biol. *17*, 732–739.

Schrier, M., Severijnen, L.A., Reis, S., Rife, M., van't Padje, S., van Cappellen, G., Oostra, B.A., and Willemsen, R. (2004). Transport kinetics of FMRP containing the I304N mutation of severe fragile X syndrome in neurites of living rat PC12 cells. Exp. Neurol. *189*, 343–353.

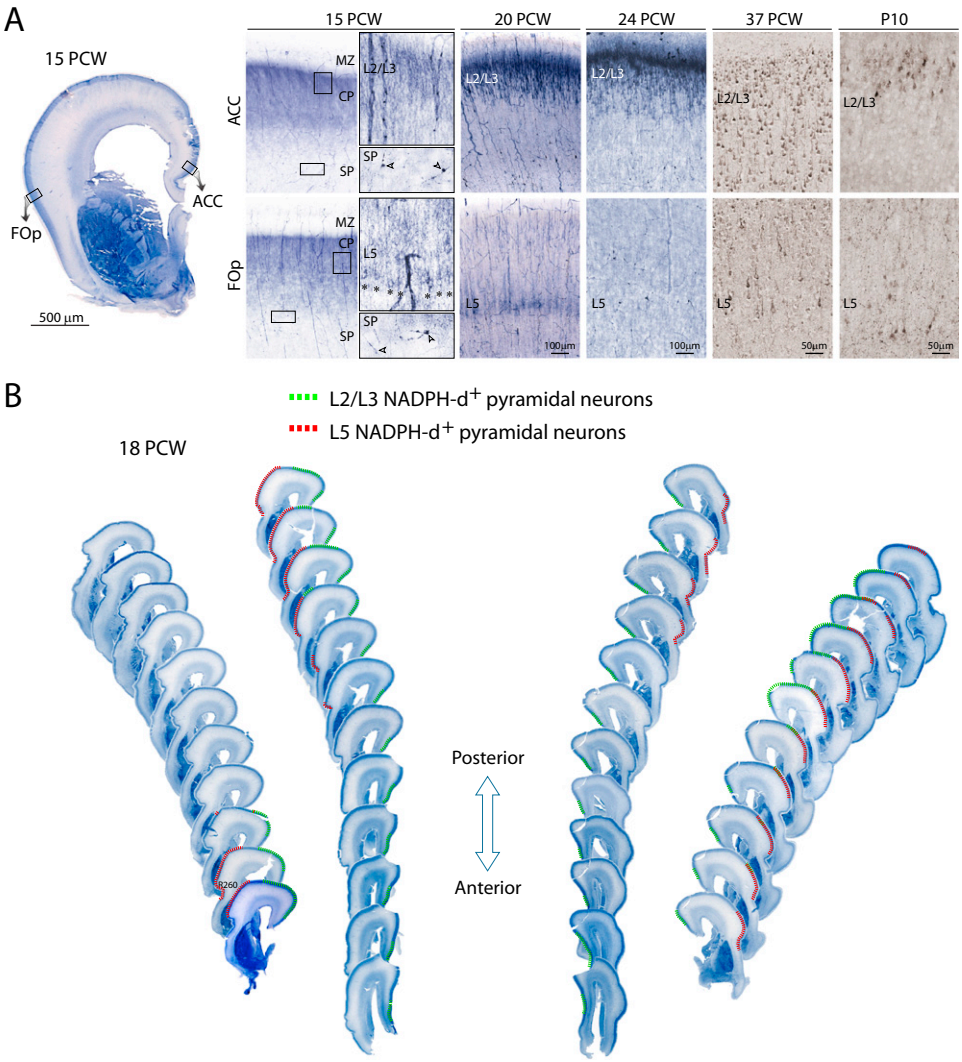

Figure S1. Spatiotemporal Expression of NOS1 in the Developing Human Neocortex, Related to Figure 1

(A) NADPH-d histochemistry (15, 20, and 24 PCW) or NOS1 immunohistochemistry (37 PCW and postnatal day (P) 10) of the human developing ACC and FOp. NADPH-d$^+$ interneurons (arrowheads) were present in the subplate (SP) as early as 15 PCW. Diffuse neuropil labeling, observed in all areas of the neocortical plate at 15 PCW, progressively decreased in the following weeks and persisted at low levels. In the ACC, intense staining of L2/L3 pyramidal neurons started at 15 PCW and persisted continuously until early infancy, when it was downregulated. In the FOp, labeling of L5 pyramidal neuron columns (asterisks) started at 15 PCW, peaked at 18-20 PCW (see also Figure 1A), and was sharply downregulated by 24 PCW. A second wave of L5 pyramidal expression occurred without apparent regional specificity or clear columnar organization in the few weeks immediately prior to birth and was downregulated during early infancy. Therefore, pyramidal NOS1 expression in the developing human neocortex was transient, and layer- and region-dependent.

(B) Bilateral distribution of NADPH-d$^+$ pyramidal neurons. One whole human fetal brain at 18 PCW was serially sectioned in the coronal plane. Every tenth section was stained using NADPH-d histochemistry. Using Stereo Investigator, the separate domains of pyramidal NADPD-d labeling in L2/L3 (green) and L5 (red) were analyzed. The domain of L2/L3 NADPH-d$^+$ pyramidal neurons started very rostrally in the ACC and was also seen more dorsally, in the adjacent dorsolateral frontoparietal cortex, in more caudal sections. In L5, NADPH-d$^+$ pyramidal neurons were positioned in the ventral part of the FOp and the most dorsal part of the anterior insula, at the rostral border of its domain. In more caudal sections, their domain shifted dorsally. Sections, both more rostral and caudal, without pyramidal NADPH-d staining were not included in the figure.

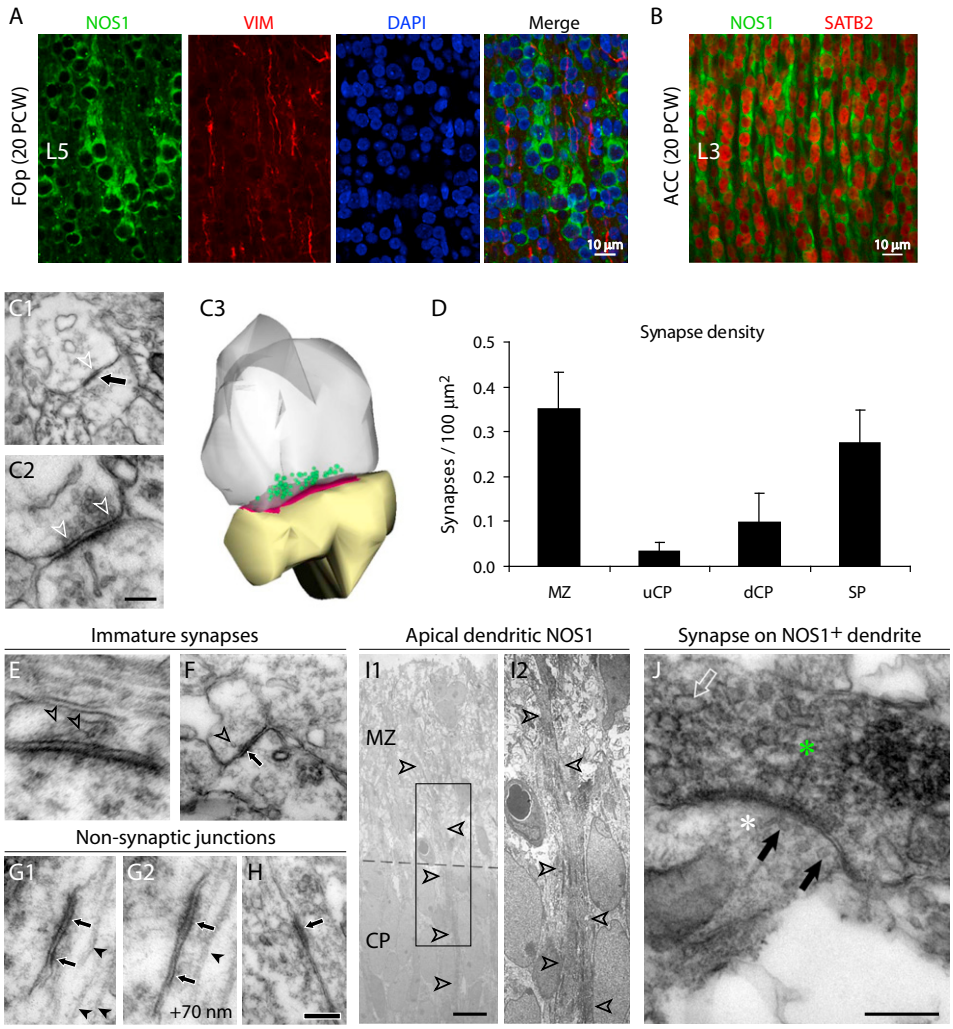

Figure S2. Analysis of NOS1$^+$ Neurons in the Human Midfetal Neocortex by Immunofluorescent Staining and Immuno-EM, Related to Figure 2

(A) Immunofluorescent staining for NOS1 (green), vimentin (VIM, red), and DAPI (blue) in L5 of 20 PCW human FOp. VIM$^+$ radial glial fibers were primarily positioned in between, but not within, the NOS1$^+$ columns.

(B) Immunofluorescent staining of NOS1 (green) and SATB2 (red) in L3 of 20 PCW human ACC. The upper layer pyramidal neuron identity of NOS1$^+$ neurons was confirmed by the expression of SATB2.

(C) Ultrastructural analysis of synapses in the 20 PCW human FOp. (C1-C2) Seventy nm thick electron microscopic (EM) micrographs of a large, asymmetric, and likely excitatory synaptic contact (black arrow). Synaptic vesicles of homogeneous size and shape were concentrated near the center of the synaptic density. Some vesicles were closely apposed to the presynaptic membrane (open arrowheads), suggesting active liberation of neurotransmitter to the synaptic cleft. This synapse was reconstructed and the axon terminal (gray), synaptic vesicles (green), postsynaptic density (red), and postsynaptic terminal (yellow) are shown in a three-dimensional view (C3). Notably, this synaptic contact, at 0.9 μm in maximum diameter, was larger than a typical adult human neocortical synapse, which averages 0.28 μm in diameter (DeFelipe et al., 2002). Scale bar represents 0.4 μm in C1, 0.13 μm in C2.

(D) Quantification of synapse density (mean ± SEM per 100 μm^2 of 70 nm thick sections) in 20 PCW FOp. The majority of synapses in the midfetal neocortex were present in the marginal zone (MZ) and subplate (SP), and only sparse synapses were present within the CP. uCP, upper cortical plate; dCP, deep cortical plate. (E and F) EM micrographs of putative developing synaptic contacts within the midfetal CP characterized by the presence of a synaptic density and vesicles heterogeneous in shape and size.

(E) A tentative axo-somatic synapse with a postsynaptic density. Large vesicle-like structures (arrowheads) were present in the presynaptic terminal.

(F) A synaptic contact (arrow) between two unidentified processes with a small number of vesicles (arrowheads) in the putative presynaptic terminal. (G and H) Nonsynaptic cell junctions in the CP.

(G) A nonsynaptic junction between a dendrite and a soma. Serial sections (G1 and G2) revealed a junction characterized by membrane thickening (arrows), regular intercellular distance, and lack of synaptic vesicles. Parallel arrays of microtubules typical of dendrites are indicated (black arrowheads).

(H) A nonsynaptic contact (arrow) between two cell somata. Vesicles were not observed on either side of the junction. Scale bar represents 0.7 μm in E, 0.14 μm in F, 0.15 μm in G, 0.26 μm in H.

(I and J) Immuno-EM reveals the presence of synapses on NOS1$^+$ dendrites. (I) NOS1 was present in pyramidal neuron distal apical dendrites (arrowheads), which extended into the MZ. (J) An example of a synapse between a nonstained process (white asterisk) with some vesicles (black arrows) and a NOS1$^+$ dendrite of unknown origin (green asterisk) in the MZ containing large vesicles (open arrow). Scale bar represents 10μm in I1, 0.13 μm in J.

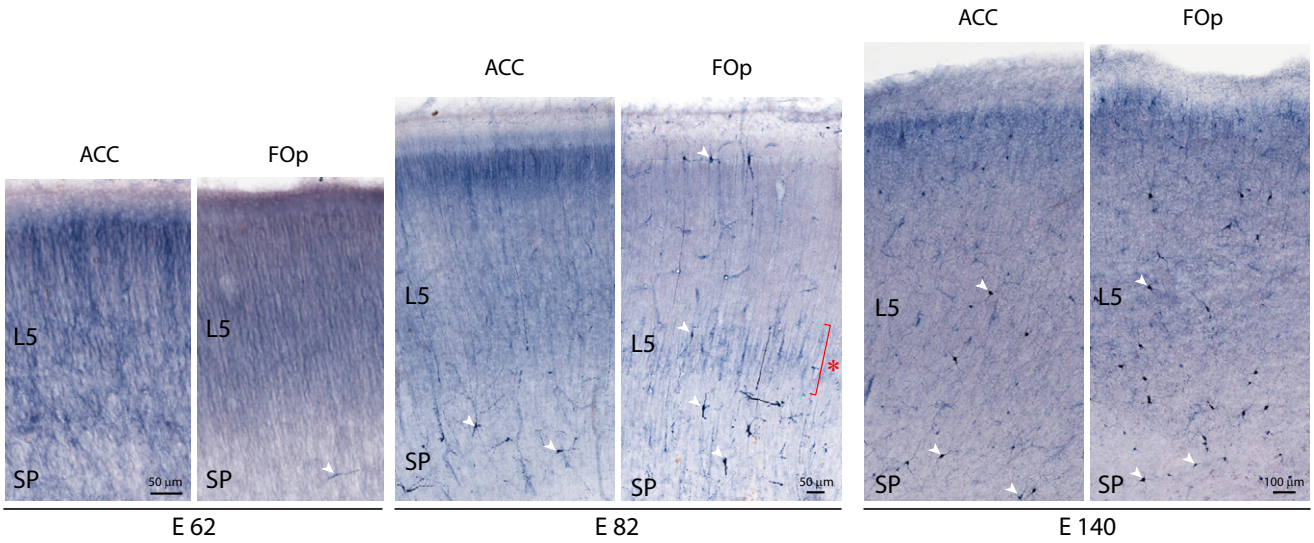

Figure S3. Spatiotemporal Expression of NOS1 in the Developing Macaque Neocortex, Related to Figure 3

The ACC and FOp of fetal macaque neocortex at E 62, E 82 and E 140 were analyzed using NADPH-d histochemistry. NADPH-d^+ interneurons (arrowheads) were observed in the subplate (SP) and CP in all areas and ages examined. Diffuse neuropil labeling, observed in all areas of the CP at E 62, progressively decreased in the following weeks and persisted at low levels. In the ACC, staining of L2/3 pyramidal neurons started at E 62 and persisted continuously until early infancy. In the FOp, labeled L5 pyramidal neurons (red asterisk) exhibited columnar organization that was present as early as E 73 (see Figure 3B), peaked at E 82, and persisted as late as E 113. Therefore, the transient, and layer- and area-dependent NOS1 expression in pyramidal neurons of the developing macaque neocortex exhibits some similarities with that of the developing human neocortex.

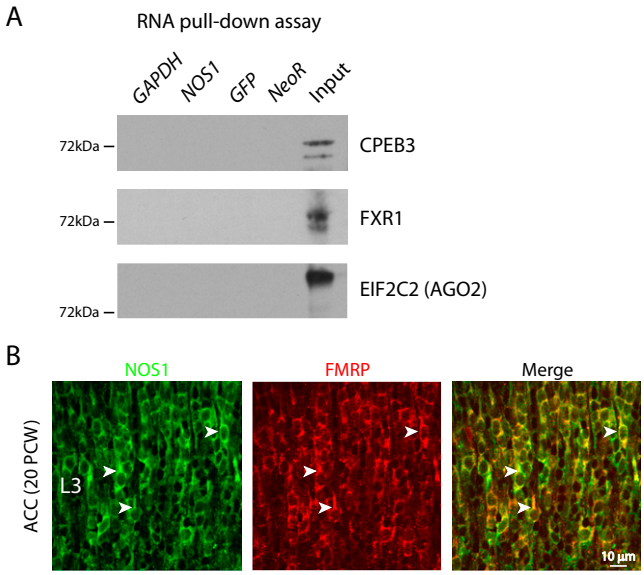

Figure S4. RNA Pull-Down Assay Immunoblots and FMRP Immunostaining in the Human Fetal ACC, Related to Figure 5

(A) RNA pull-down assays were carried out using full-length RNAs of *GAPDH*, *NOS1*, *GFP* and *NeoR* and lysates from human 21 PCW neocortex. Bound proteins were analyzed by immunoblotting. Unlike FMRP (see Figure 5A), CPEB3, EIF2C2, and FXR1 were not significantly pulled down by any of the RNAs.

(B) NOS1$^+$ L3 pyramidal neurons in the ACC co-express FMRP. Immunofluorescent staining of NOS1 (green) and FMRP (red) in L3 of 20 PCW human ACC. The NOS1$^+$ pyramidal neurons of the midfetal ACC, which did not display clear columnar organization, expressed high levels of FMRP (arrowheads).

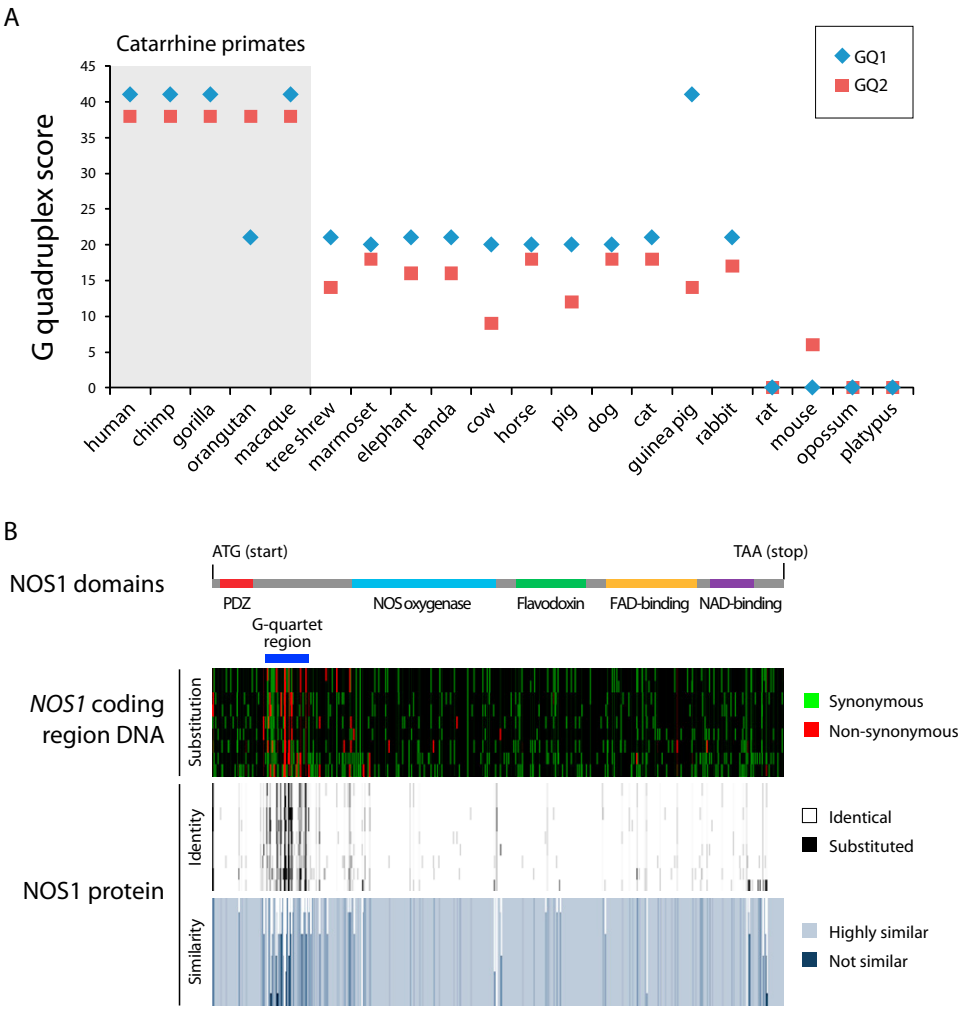

Figure S5. Evolution of *NOS1* G-Quartet Sequences, Related to Figure 6

(A) GQ prediction in mammalian *NOS1* sequences orthologous to human GQ1 and GQ2 in nineteen placental mammals, one marsupial, and one monotreme. G quadruplex scores were calculated using QGRS Mapper (Kikin et al., 2006).

(B) DNA and amino acid sequence alignment of the coding region of *NOS1* in nine mammals. The *NOS1* coding sequences of human, chimp, elephant, panda, horse, cow, dog, rabbit, mouse were aligned using ClustalW. At the DNA level, synonymous substitutions (green), mostly the result of silent third base pair wobbles, were distributed over the entire coding region whereas nonsynonymous substitutions (red) were clustered near the GQ region. Correspondingly, at the protein level, amino acid substitutions, especially dissimilar substitutions, preferentially accumulated within the GQ region.

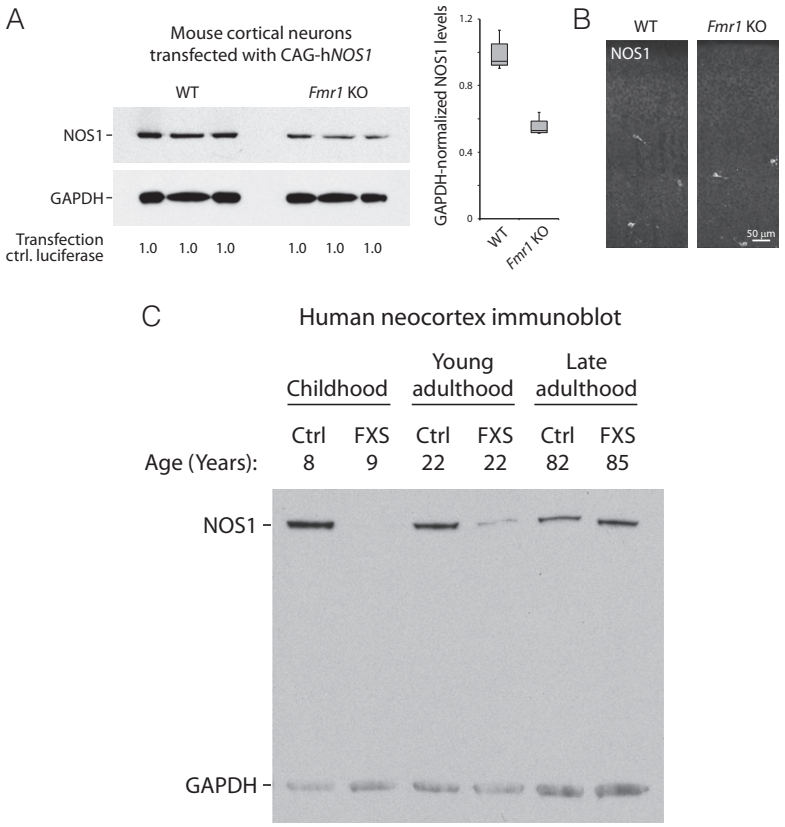

Figure S6. Exogenous Expression of Human *NOS1* in Mouse Neurons and NOS1 Expression in Mouse *Fmr1* Knockout and Human Fragile X Syndrome Brains, Related to Figure 7

(A) NOS1 immunoblots of mouse neurons cultured from E14.5 wild-type and *Fmr1* knockout (KO) neocortex co-transfected with CAG-human *NOS1* (CAG-h*NOS1*) and a transfection control luciferase. Lysates containing equal amounts of luciferase activity were immunoblotted. Compared to wild-type, NOS1 protein expression in *Fmr1* KO neurons was significantly decreased (43.8 ± 7.8% reduction, *p = 0.0065).

(B) Immunostaining of endogenous NOS1 in wild-type and *Fmr1* KO P0 neocortex. The expression of endogenous NOS1, which was restricted to interneurons in the mouse neocortex, was not affected in the *Fmr1* KO.

(C) NOS1 expression in the postnatal fragile X syndrome (FXS) neocortex. Dissected frontal neocortex of confirmed postnatal FXS cases and age-matched controls was analyzed for NOS1 expression by immunoblotting. Lysates were normalized using *GAPDH* levels. In the childhood (9 years) FXS neocortex, NOS1 was dramatically reduced compared to control. This reduction was less severe in the young adult (22 years) FXS neocortex. In the aged adult (85 years) FXS neocortex, NOS1 levels were comparable to control.